*Polymers* **2014**, *6*, 2473-2509; doi:10.3390/polym6092473

OPEN ACCESS

*polymers*

**ISSN 2073-4360**

www.mdpi.com/journal/polymers

*Review*

# Towards High Performance Organic Photovoltaic Cells: A Review of Recent Development in Organic Photovoltaics

**Junsheng Yu *, Yifan Zheng and Jiang Huang**

State Key Laboratory of Electronic Thin Films and Integrated Devices,
School of Optoelectronic Information, University of Electronic Science and Technology of China (UESTC),
Chengdu 610054, China; E-Mails: 382297472@163.com (Y.Z.); huangjiang@uestc.edu.cn (J.H.)

* Author to whom correspondence should be addressed; E-Mail: jsyu@uestc.edu.cn;
Tel.: +86-28-8320-7157; Fax: +86-28-8320-6123.

*Received: 28 July 2014; in revised form: 16 September 2014 / Accepted: 19 September 2014 / Published: 25 September 2014*

---

**Abstract:** Organic photovoltaic cells (OPVs) have been a hot topic for research during the last decade due to their promising application in relieving energy pressure and environmental problems caused by the increasing combustion of fossil fuels. Much effort has been made toward understanding the photovoltaic mechanism, including evolving chemical structural motifs and designing device structures, leading to a remarkable enhancement of the power conversion efficiency of OPVs from 3% to over 15%. In this brief review, the advanced progress and the state-of-the-art performance of OPVs in very recent years are summarized. Based on several of the latest developed approaches to accurately detect the separation of electron-hole pairs in the femtosecond regime, the theoretical interpretation to exploit the comprehensive mechanistic picture of energy harvesting and charge carrier generation are discussed, especially for OPVs with bulk and multiple heterojunctions. Subsequently, the novel structural designs of the device architecture of OPVs embracing external geometry modification and intrinsic structure decoration are presented. Additionally, some approaches to further increase the efficiency of OPVs are described, including thermotics and dynamics modification methods. Finally, this review highlights the challenges and prospects with the aim of providing a better understanding towards highly efficient OPVs.

**Keywords:** organic photovoltaic cell (OPV); OPV structure design; annealing treatment; photophysics mechanism; additives

---

## 1. Introduction

Photovoltaic (PV) technology, which allows the generation of electricity directly from sunlight, is expected to play a major role in solving the global energy crisis in an environmentally-friendly and sustainable way. The future success of PVs will rely on advances in material research and the cell design concept to increase device efficiency and stability, as well as to reduce the manufacturing, installation and operational costs [1]. At the current stage, the PV market relies heavily on wafer-based polycrystalline silicon devices and various inorganic materials, including silicon, CdTe, GaAs, $CuIn_xGa_{1-x}Se_2$-based thin film PVs, are the dominating technologies on the market [2–6]. However, conventional PV technology with a high production cost and related environmental issues has not successfully replaced grid electricity, and the electricity generated from PV only accounts for less than 0.1% of the total worldwide energy generation [7]. In last few decades, there has been an unabated continuous interest in organic photoelectronic technology, including organic light-emitting devices (OLEDs) and organic photovoltaic cells (OPVs), which are due to their synthetic variability, low cost fabrication process and the great potential to produce flexible, easily manufactured devices [8–12]. So far, OLEDs for display and solid state lighting have been commercialized, and in comparison, OPV has been improved from a fancy concept with less than 1% power conversion efficiency (PCE) to over 10% PCE to meet the requirement of the PV marketplace [13].

A key difference between organic and inorganic PVs is the relative importance of interfacial processes. The primary goal in almost all solar energy conversion systems is the utilization of incident solar energy to generate separated electronic charges [14]. Efficient energy transduction requires the charge carrier of the electron and hole to overcome their mutual Coulomb attraction $V$, which can be quantified by Equation (1):

$$V = \frac{e}{4\pi\varepsilon_\gamma\varepsilon_0\gamma} \tag{1}$$

where $e$ is the charge of an electron, $\varepsilon_\gamma$ is the dielectric constant of the surrounding medium, $\varepsilon_0$ is the permittivity of vacuum and $\gamma$ is the electron-hole separation distance. In conventional inorganic PVs, overcoming Coulomb attraction is facile, due to the high constant of inorganic materials (e.g., silicon, $\varepsilon_\gamma \approx 12$, $TiO_2$, $\varepsilon_\gamma \approx 80$). However, in OPVs, the smaller dielectric constant ($\varepsilon_\gamma \approx 2$–4) and more localized nature of the electronic states cause photoexcited states to be confined to a small volume (few $nm^3$) in space and create a large Coulombic barrier (0.1–1 eV) to dissociating into separate electrons and holes [15]. Moreover, the inter-molecular charge transport is much more difficult for organic materials than their inorganic counterparts. The low charge mobility of organic materials, due to the localization of charged states, is associated with the high possibility of charge recombination [16]. Furthermore, organic materials usually show an exciton diffusion length of ~10 nm and optical absorption depths of 100 nm [17–19]. The thickness of the active layer range from 30 to 100 nm in order to efficiently collect the photogenerated carriers, which is too thin to capture the incident light accordingly. Hence, various exploits in device architecture and processing techniques, as well as further understanding of the OPV functioning mechanism all make contributions toward achieving high PCE.

From their very beginning, the OPVs were simple, single-layer devices based on a Schottky diode structure, a pristine polymer and two electrodes, resulting in low PCE [20–22]. The first relatively

successful OPV was reported by Tang *et al.* in 1986, which was based on a double-layer structure of p-type copper phthalocyanine and n-type perylene diimide derivative [23]. It was found that the use of a heterojunction consisting of two different organic semiconductors with offset energy levels, the donor (D) and acceptor (A) is effective at separating the tightly bound exciton. $D^+/A^-$ charge-transfer (CT) states are more energetically favorable than the exciton state of either D or A. In the early 1990s, Heeger *et al.* observed the ultrafast photo-induced electron transfer from a conjugated polymer to $C_{60}$, and the consequent enhancement in charge photogeneration yield opened up the potential of using solution-processed polymers in OPV [24–26]. However, the short exciton diffusion length requires the thickness of the active layer to be thin enough, which, in turn, impedes light absorption. In this case, in 1992, a bulk heterojunction (BHJ) structure was employed to overcome the primary issue in double-layer OPVs [27,28]. The bicontinuous interpenetrating network of D–A in the BHJ structure provides a large area for exciton dissociation and, thus, reduces the length of separated excitons to the corresponding electrodes. The founding of BHJ is a milestone in the progress of OPV, in that it greatly renders the improvement of PCE of OPVs. From there on, BHJ has become a typical structure for OPVs, and further works on improving the performance of OPVs are mainly based on this device architecture framework.

In last few decades, many works have been carried out on the illumination of the working mechanism of OPVs, the inventory of simple and efficiency processing techniques, the exploration of novel OPV architectures and to increase the device stability, design and synthesis of new materials, which are all working towards improving the PCE of OPVs [29–38]. To date, the highest reported PCEs are in the range of 6.7%–8.94% for small molecule [39–41], 8.4%–10.6% for polymer OPVs [42–44] and 7%–15% for perovskite OPVs [45–47]. The recent developments in OPVs open the way toward low-cost, environmentally-benign and renewable power sources.

Herein, the main purpose of this work is to guide the reader by capturing brief information regarding state-of-the-art OPVs. This review paper takes a retrospective look at the research and development of OPV in the last five years, especially in the understanding of the developed theoretical interpretation, the novel designs of the device architecture and the newly preferentially modifications. Due to space limitation, we mainly focus on the study of the active layer. Works on the hole transport layer (HTL) and electron transport layer (ETL) will not be discussed here, which also play a critical role in OPV performance.

## 2. Photophysics Mechanism

### *2.1. Hot Exciton Dissociation*

OPVs use a single heterojunction between the donor (D) and acceptor (A) semiconductors to generate charge carrier. The state-of-the-art polymer cells are cast from a solution of D:A mixture with nanoscale domains and large interfacial regions [27]. This architecture is well known as the BHJ. The key photophysical processes in an OPV are displayed in Figure 1.

In the first step, the absorption of sunlight in the bulk domains forms singlet excitons with different energy, referred to as $S_0 \rightarrow S_n$. Then, the high energy level of singlet excitons will diffuse at a short distance of about tens of nanometers to the D/A interface, where offsets between the LUMOs (lowest unoccupied molecular orbitals) of D and HOMOs (highest occupied molecular orbitals) of A enable

electron transfer, thereby dissociating the singlet excitons. As presented in Figure 1, the ultrafast energy transfer process from $S_n$ of the polymer domain to the temperate states of the polymer/fullerene mixing phase will happen within several tens of femto-seconds, yielding the hole on D and the electron on A. Due to the low dielectric constant of these materials ($\varepsilon_\gamma$ within 3–4), the charges remain electrostatically attracted across the D/A interface with length scales smaller than the Coulomb capture radius $r_c = e^2/4\pi\varepsilon_0\varepsilon_\gamma k_B T$ at room temperature [48,49], leading to a high rate of electron-hole encounters. That could produce Coulombic bound "charge-transfer" CT states with the binding energies of several hundred meV [50], without consideration of whether these states eventually dissociate into free carriers or stay bound until recombination [51]. The fundamental question is how the organic heterojunction enables efficient long-range charge separation, especially; some OPV systems work very efficiently with internal quantum efficiency to 100% [52].

**Figure 1.** (**a**,**b**,**c**) Calculated excited-state energy levels for poly(2,6-(4,4-bis-(2-ethylhexyl)-4*H*-cyclopenta(2,1-b;3,4-b')-dithiophene)-*alt*-4,7-(2,1,3-benzothiadiazole)) oligomer featuring four repeat units (CPDTBT4), CPDTBT4/[6,6]-phenyl-C61-butyric acid methyl ester ($PC_{60}BM$) and $PC_{60}BM$ and the computed interfacial exciton state (IES), density of state (DOS) and sketch of the molecular dimer; Cited from [53]. Copyright 2013, Nature.

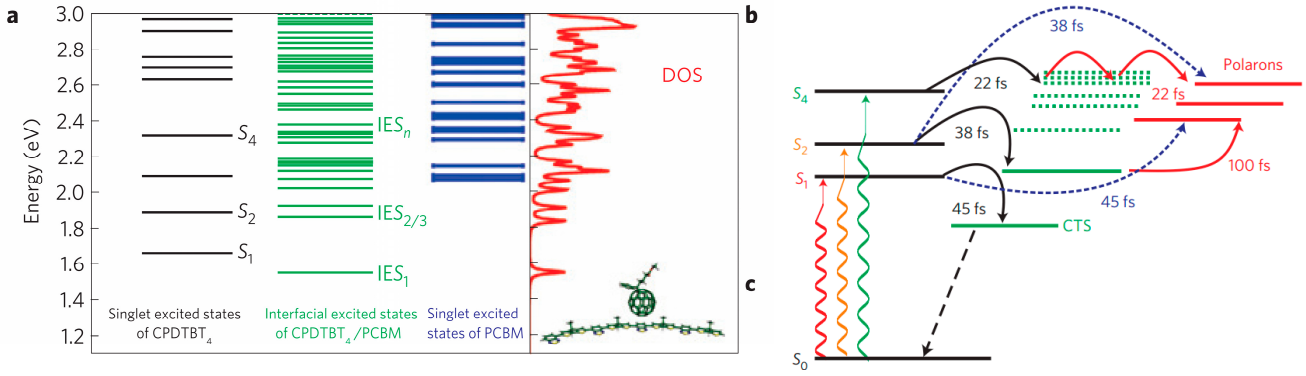


The density of states in the poly(2,6-(4,4-bis-(2-ethylhexyl)-4*H*-cyclopenta(2,1-b;3,4-b')-dithiophene)-*alt*-4,7-(2,1,3-benzothiadiazole)) oligomer featuring four repeat units (CPDTBT4)/[6,6]-phenyl-C61-butyric acid methyl ester ($PC_{60}BM$) heterojunction is directly detected and confirmed by calculation by Lanzani *et al.* Their work clearly disclosed singlet excitons $S_4$ with higher energy directly from $CT_n$ with a higher level than the lowest $CT_0$ [53]. Before $CT_n$ cool down to $CT_0$, they have additionally enough "excess energy" inherited from $S_4$ to form a polaron hole in polymer and free electron in fullerene within 22 fs. Meanwhile, the lower CTs formed from singlet excitons $S_1$ and $S_2$ have less excess energy and can only partially dissociate into polarons with a much longer lifetime ~100 fs. Finally, most of them cool down to $CT_0$, and decay to the ground state through both radiative and nonradiative recombination.

The inherited "excess energy" from the higher energy of excited states associating with the charge dissociation at the D/A interface has been well known as the hot exciton dissociation process in the OPV system [54,55]. The ultrafast hot exciton dissociation significantly contributes to photocurrent when absorbing low wavelength photons. The CTs are more delocalized in nature and, thus, more prone to ultrafast charge separation instead of relaxation to the bound $CT_1$ state, which constitutes a loss path,

due to a stronger coupling to the ground state. The excess energy of hot $CT_n$ states has been considered to be lost during relaxation to the "cold" $CT_0$ state, facilitates long-range charge separation [54,55].

Friend's group used additional infrared (IR) photons to promote the cooled $CT_0$ to higher energy level $CT_n$, as shown in Figure 2 [56]. From the pumped and decay photocurrent, the cooling process from $CT_n$ to $CT_0$ and dissociation dynamic from $CT_n$ to separated charge (SC) are investigated in both polymer/fullerene and polymer/polymer systems. Transient measurements indicated that the "excess energy" of the hot CT state was ~0.5 eV higher than that of the low energy CT state from cross-section $S_0 \rightarrow$CT. Thus, the photocurrent gains were similar for sub- and above-gap excitations, demonstrating that charge separation effectively occurred without needing a large amount of excess energy. In contrast, they proposed that the role of driving energy has close dependence on the general trend of the delocalization of charge by optical excitation. The extent of delocalization is material dependent, *i.e.*, moving from poly(9,9-dioctylfluorene-*co*-benzothiadiazole) (F8TBT) to $PC_{60}BM$ with the increase of average electron-hole separation by 50%, as shown in Figure 2. This, in turn, induces even larger variation in CT state binding energy and dissociation probability. This difference in the delocalization of charges causes OPV systems to demonstrate remarkably different quantum efficiencies. Furthermore, their study is crucial for guiding the material designation of both the polymer donor and non-fullerene acceptor.

**Figure 2.** Micro-electrostatic simulations of the charge distribution at the poly-3(hexylthiophene) (P3HT)/$PC_{60}BM$ (**A**,**B**) and P3HT/F8TBT poly(9,9-dioctylfluorene -*co*-benzothiadiazole) (**C**,**D**) heterojunction, with electron and hole densities shown in blue and red, respectively. (**A**,**C**) Charge distribution in the lowest CT-state configuration and (**B**,**D**) in the excited CT state configuration created upon absorption of an IR-push photon. R, average electron-hole separation. Cited from [56]. Copyright 2012, Science.

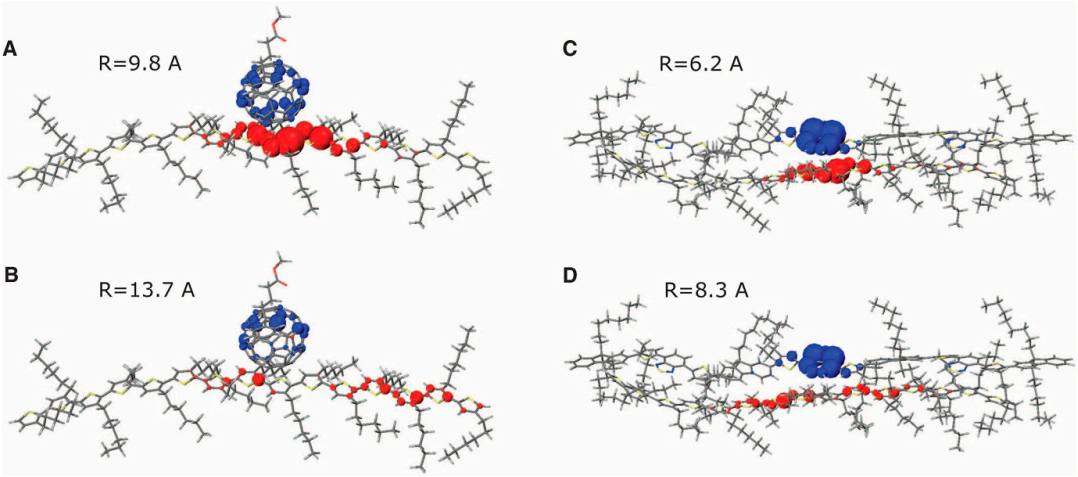


*2.2. Spin Nature of CT States*

To overlap a greater range of the solar light spectrum and to absorb more photons, the optimized optical energy band of the polymer is around 1.5 and 1.7 eV, which can generate $J_{SC}$ from 15 to 22 mA/cm$^2$. Nowadays, the state-of-the-art OPVs with high PCEs of about 8.8% and 9.2%, reported from Yang *et al.* and Cao *et al.* [57,58], respectively, with $J_{SC}$ and internal quantum efficiency almost near 100%, corresponding to ultrafast charge dissociation and charge collection efficiencies. In terms of

$V_{OC}$, it is well established that the open-circuit voltage ($V_{OC}$) is determined by the energy difference between the HOMO level of D and the LUMO level of A, and lower HOMO donors or higher LUMO acceptors have attracted a great amount of attention. Thus, the optimizing capability of POV performance becomes less due to the trade-off between $V_{OC}$ and $J_{SC}$. The critical fundamental question is whether we can repress the "excess energy" of CT states to less than 0.3 eV to obtain a larger gain in $V_{OC}$ while maintaining $J_{SC}$. Unfortunately, the attempts to challenge this have not yet succeeded.

A typical example is the trade-off using donor copolymer poly(indacenodithiophene-*co*-phenanthro quinoxaline) (PIDT-PhanQ) [9,10] synthesized by Jen's group [59,60]. From Figure 3, we can obviously see that the OPV with the PIDT-PhanQ/(6,6)-phenyl-C71-butyric acid methyl ester ($PC_{70}BM$) heterojunction has the highest $J_{SC}$ and fill factor (FF). However, when using higher LUMO fullerene, *i.e.*, indene-C60 bisadduct ($IC_{60}BA$) and indene-C70 bisadduct ($IC_{70}BA$), although the $V_{OC}$ was effectively enhanced from 0.8 V to near 1 V, the $J_{SC}$ and FF obviously decreased, which was ascribed to additional energy loss paths [59]. This phenomenon is commonly observed in other polymer systems and, thus, cannot be simply explained by the lower "excess energy" of CT states [61].

**Figure 3.** (**a**) Schematic depiction of solar cell structure employed here, consisting of a blended polymer fullerene active layer with poly(indacenodithiophene-*co*-phenanthro quinoxaline) (PIDT-PhanQ) as the donor; (**b**) photocurrent density as a function of voltage for the device structure in (**a**) using fullerenes 1–4 as acceptor materials, measured under simulated Air mass (AM) 1.5 G solar illumination at 1 $kW \cdot m^{-2}$. Cited from [59]. Copyright 2012, America Chemical Society.

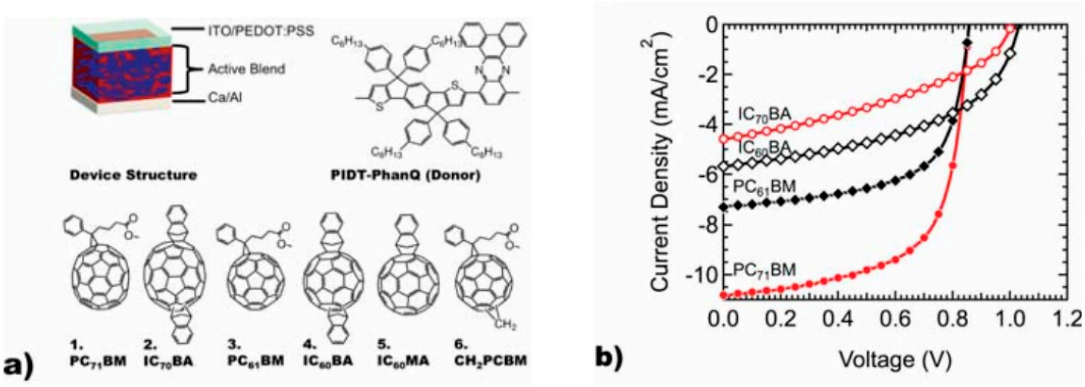


Friend's group studied the actual energy loss paths and also the spin nature of CT states in the D/A system, and their investigation opened the fundamental understanding about the triplet CT states and their functions in the photovoltaic process [62]. As shown in Figure 4, the singlet exactions are firstly generated in the bulk of donor and acceptor (Process 1). Singlet excitons diffuse to the D/A interface, and singlet CT states ($^1$CT) form and separate into free charges (FC) (Process 2). The hole-electron of FC is banded together due to bimolecular recombination forming 1/4 $^1$CT and 3/4 triplet CT states ($^3$CT) (Process 3). Herein, the formed $^1$CT state can recombine to the ground state via both nonradioactive and radioactive recombination process that can be reorganized in the photoluminescent (PL) spectrum (Process 6). As for the $^3$CT state, relaxation to the triplet exciton ($T_1$) state of the donor (or acceptor) is more energetically favorable than recombination to the ground state due to spin-forbidden states

(Process 4). The increased population of triplet excitons leads to stronger phosphorescent PL density through an efficient triplet-charge annihilation channel (Process 5).

Due to the energy of the CT state being higher than that of the $T_1$ state in the PIDT-PhanQ blends, the evolution of CT states to free charges and back transfer to a singlet or triplet exciton can be easily distinguished. For the PIDT-PhanQ/$PC_{60}BM$ system, there is no characteristic spectrum of triplet exciton in the transient absorption spectra, indicating that energy transfer from CT states to triplet excitons is forbidden at room temperature. However, triplet excitons are generated in the PIDT-PhanQ/$IC_{60}BA$ system, indicating a major energy loss path of CT states. Due to the triplet-charge annihilation, the triplet excitons would immediately decay to the ground state. The completion between the triplet $^3$CT state to free charges with transition time $\tau_3$ and $^3$CT to triplet excitons with transition time $\tau_4$ determines the quantum efficiency of final photocurrent generation. At a high temperature (>240 K), $\tau_4 > \tau_3$ means efficient $^3$CT states to free charges. At a lower temperature, this dissociation process is suppressed, $\tau_4 < \tau_3$, leading to back transfer from $^3$CT states to triplet.

**Figure 4.** State diagrams representing the various photophysical processes in an OPV. Conversions between excited state species are shown in blue, and recombination channels are shown in red. Cited from [62]. Copyright 2013, Nature.

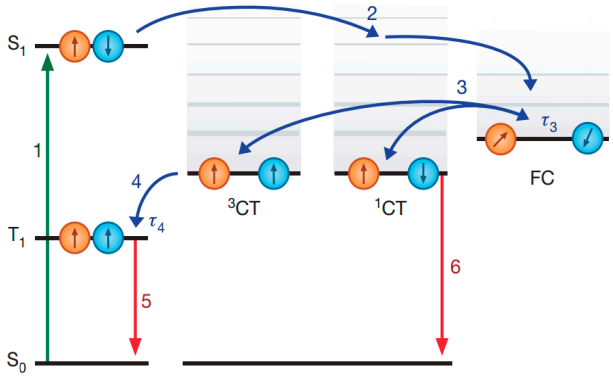


Another fundamental question is why the PIDT-PhanQ/$PC_{60}BM$ system has unique characteristics. It is known that, in contrast to other fullerenes, $PC_{60}BM$ forms large aggregates more efficiently. A larger aggregation domain aids charge separation [63]. They found that triplet emission was enhanced due to the transition from $^3$CT states to triplet excitons when decreasing the $PC_{60}BM$ ratio. This promoted further study on the relationship between the fullerene aggregation size and their electron wave functions.

### *2.3. Charge Separated States*

As presented above, the domain size of fullerene aggregates greatly influences the charge dissociation time $\tau_4$. A small domain size would result in $\tau_4 < \tau_3$, leading to energy transfer from CT states to triplet excitons [62]. Marks' group then made a calculation of the fullerene cluster and obtained interesting results [64]. In some material systems, all of the charge separated (CS) states can be remarkably collected as electrical current [65]. While in other systems, a large fraction of CS states are short-lived and recombine on similar time scale to the singlet excitations, which refers to lower energy CT states [66–68], Additionally, their occurrence has been empirically connected with poor

morphology [69,70]. At a higher fullerene-to-polymer ratio, a larger domain size of fullerene can be formed. Thus, resonant CS states are abundant, and CT states should play a minimal role (Figure 5). They proposed that exciton delocalization in the polymer main chain may not be necessary for efficient charge generation, compared with the CS states formed from the aggregation of fullerene. If exciton delocalization in the donor were the primary determinant of charge generation efficiency, then geminate losses should be correspondingly independent of the acceptor used in the device. Furthermore, most of the D/A OPV systems are strongly dependent on the fullerene ratio. Their electronic structure calculations on the large clusters of functionalized fullerenes is well consistent with the transient pump-push-photocurrent data, which predicts several features of charge generation process, outside the framework of conventional theories, *i.e.*, Onsager theory [71–73] and Marcus theory [74,75].

**Figure 5.** Fundamental charge generation processes, morphology, and device configuration in bulk-heterojunction organic photovoltaics: (**a**) Schematic depiction of the currently accepted bulk heterojunction microstructure with $PC_{60}BM$ acceptors (blue spheres) and polymer donors (gold strands) present with varying degrees of order and mixing; (**b**) Typical device configuration with the active layer (green) sandwiched between metallic and transparent electrodes. Interfacial layers (blue and gold) are chosen for selective extraction of electrons or holes. The states relevant to charge generation in (**c**) polymer:fullerene blends and (**d**) typical nonfullerene acceptor blends. Excited states (blue) predominantly occur in the donor phase with time-dependent localization and thermalization. In each case, the DOS accessible at the donor−acceptor heterojunction is depicted. In blends of fullerene (**c**), isoelectronic states resonant with the donor exciton facilitate charge generation directly. In nonfullerene blends (**d**), there is minimal accessibility to isoenergetic CS states, except through long-range tunneling or a Coulombically trapped intermediate. In each case, low-energy states are localized near the heterojunction and stabilized by the electron−hole Coulombic interaction. $k_{CS}$ refers to the rate of CT to unbound CS, $k_{CT}$ is the rate of CT to the low-energy CT, and $k_R$ is the rate of recombination. Cited from [64]. Copyright 2014, America Chemical Society.

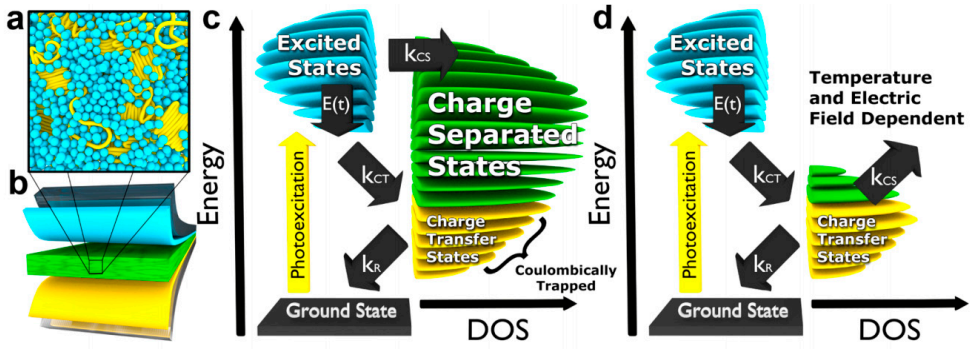


## 3. OPV Structure Design

In 1986, Tang *et al*. pioneered the donor-acceptor double-layer planar heterojunction to OPV cells with a PCE of around 1% [23]. Following this breakthrough in OPV cells was the adoption of $C_{60}$ fullerene and its derivative, $PC_{60}BM$, demonstrating the planar heterojunction OPVs in 1993 [26].

The simple layer-to-layer structure is the widest applied in OPV cells with a double-layer planar heterojunction, which is convenient for controlling in the vacuum evaporating system with high repeatability. However, the planar junction concept has certain shortcomings, including a small surface area between the donor-acceptor interface and the requirement of a long carrier lifetime to ensure that the charge carriers move to the corresponding electrodes [12]. In this case, BHJ was introduced to provide the larger D/A interface, which was firstly reported by Heeger and Friend [28]. A BHJ material is a solid state mixture of two components, D and A, with a nanostructured morphology formed by spontaneous phase separation: these D and A components self-assemble to form bicontinuous interpenetrating networks. Figure 6 shows the conventional device architecture of BHJ OPVs. The formation of interpenetrating networks requires the phase separation of component materials, in which the interfacial energy favors a large surface area and that each of the two components is fully percolated with connected pathways to the electrodes [76–78]. An "ordered bulk heterojunction", consisting of vertically aligned conjugated polymer nanorods surrounded by the electron acceptor materials to form the ordered bicontinuous heterojunction morphology for the active layer, yet achieving this morphology, has been elusive [79,80].

**Figure 6.** Conventional device architecture of the bulk heterojunction solar cells. Cited from [78]. Copyright 2014, Wiley.

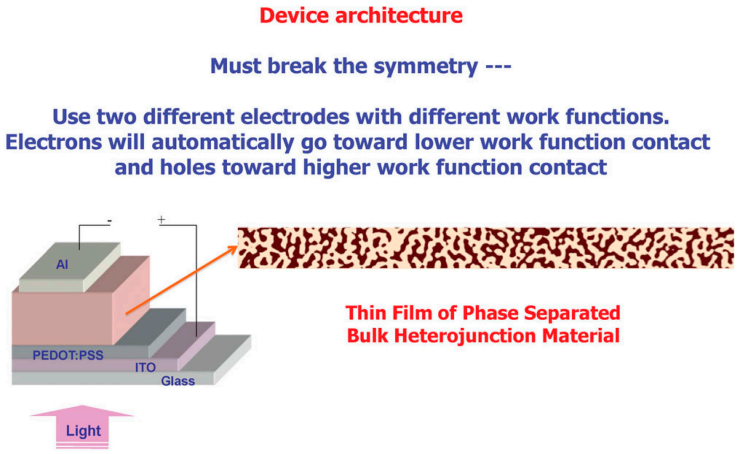


It is difficult to control and characterize the non-equilibrium morphology of BHJs, and the reason is as follows. Firstly, the BHJ structure is usually prepared by spin-casting from a volatile solvent, which is very sensitive to solvent quality, evaporation rate, solution concentration, ambient temperature and moisture [81]. Secondly, the BHJ growth kinetics is controlled by a coupled crystallization-diffusion mechanism, so the key parameters, such as domain size, phase purity and polymer crystallinity, cannot be varied independently [82]. Thirdly, the disorder and anisotropy of the BHJ morphology at both molecular and nanometric length scales make it difficult to characterize through scattering and microscopy [83]. The design of the OPV structure may provide a new opportunity to overcome the bottleneck of BHJ for the significant improvement of PCE.

Several groups have used nanoimprint lithography to produce the polymer nanostructures by using a Si mold, leading to an increase of fabrication cost [84,85]. An anodic aluminum oxide (AAO) membrane is another widely used templates for the fabrication of polymer-based nanostructures, including nanotubes, nanorods, mesoporous nanostructures and vesicles [86–89].

However, imprint lithography has a couple of disadvantages. Firstly, master stamp fabrication is expensive and difficult, especially for large-scale OPV. Secondly, different designs for imprint lithography can be costly and time-consuming. Thirdly, the imprinted nanostructure has limited stability through solvent processing or heat treatments. Finally, the polymer crystallinity and grain orientations should be taken into consideration in the stamp design, due to the imprinted nanostructure inducing the alignment of the polymer chains within the template.

Recently, P3HT nanopillars have been fabricated by using AAO [90,91]. However, the basic or acidic solution used to remove the template will react with P3HT, deleteriously affecting the device performance [92]. In this case, Chen *et al.* presented a simple, cost-effective method for the fabrication of P3HT nanopillars by using PDMS to reduce the surface energy of AAO templates [93]. The procedure for the nanostructured OPV is shown in Figure 7. The PCE of OPV based on P3HT nanopillars was significantly improved from 0.82% to 2.4%.

**Figure 7.** Procedure for the nanostructured organic photovoltaic device. Cited from [93]. Copyright 2012, America Chemical Society.

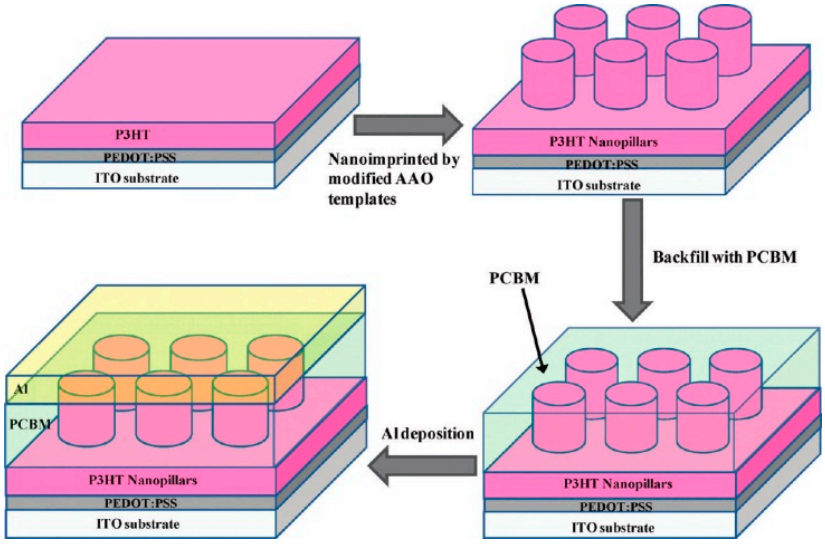


Moungthai *et al.* reported a simple approach to control the morphology of P3HT/$PC_{60}$MB OPV based on the electron-beam pattering of polymer semiconductors, as shown in Figure 8 [94]. By directly patterning the P3HT with electron-beam lithography, a conductive nanostructure or microstructures could be obtained. Polymers with a cross-linked structure are resistant to heat and solvent. Therefore, they can be incorporated into devices for thermal annealing or solution-based processing. Cross-linked structures are very valuable for the fundamental structure-property investigation, since the nanostructure size, shape, density and placement are all controlled with computer software. Compared with the conventional BHJ devices, patterned P3HT films with a larger P3HT/PCBM interfacial area are conducive to the generated charge.

Tao *et al.* reported a crosslinking process for P3HT and applied it to the fabrication of planar and patterned BHJ OPVs, as shown in Figure 9 [95]. The results of neutron reflectometry and XPS demonstrated that PCBM could percolate throughout the crosslinked P3HT and form the intermixed network. Pillars with feature sizes down to 2 μm were produced, and after subsequent deposition of PCBM and thermal annealing, devices with efficiencies of up to 1.4% were obtained. The crosslinking

process can lead to well-defined patterned films, and these structure films can give rise to OPVs in which efficiency is directly related to the amount of P3HT that remains.

**Figure 8.** Direct patterning of gradient (**top**) and nanostructured (**bottom**) polymer/fullerene solar cells. ITO (indium tin oxide); PEDOT:PSS (poly(3,4-ethylenedioxythiophene): poly-(styrenesulfonate)); P3HT (poly(3-hexylthiophene), PCBM ((6,6)-phenyl-$C_{61}$-butyric acid methyl ester). PCBM is spin-cast from dichloromethane (DCM). Cited from [94]. Copyright 2012, America Chemical Society.

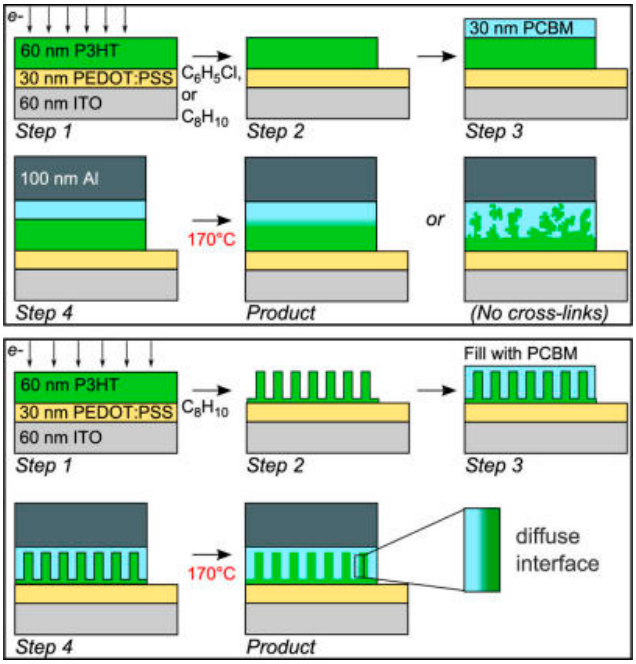


**Figure 9.** Photographs (**a**–**c**) of patterned crosslinked P3HT films on glass/ITO/PEDOT:PSS substrates following deep-ultraviolet light (DUV), 254 nm wavelength exposure and solution development; (**d**) 3D AFM (atomic force microscope) image of 2-μm pillars in a patterned crosslinked P3HT film. Cited from [95]. Copyright 2013, Wiley.

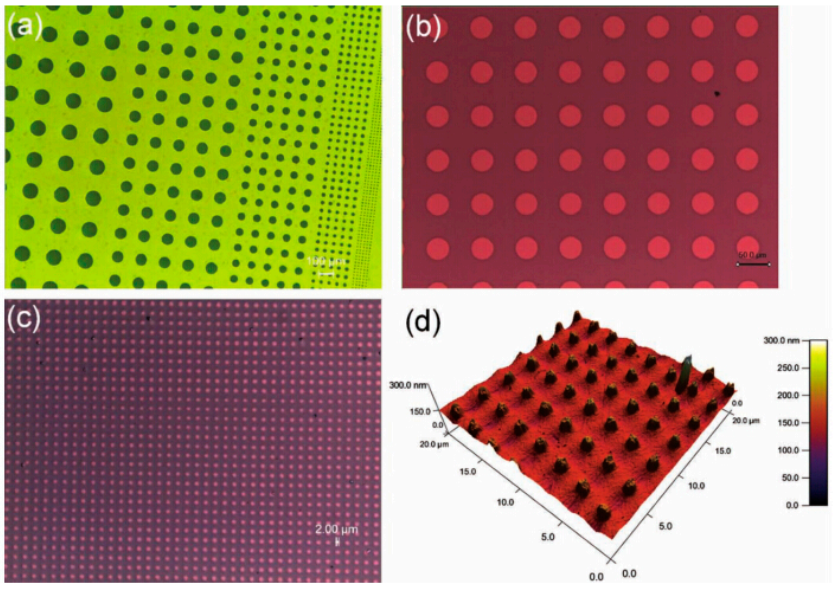

In addition to the crosslink structure, a novel design of OPV has been focused on the investigation of a novel device structure to capture more light. Loo *et al.* exploited a wrinkled and deep fold form on the polymer surface when subjected to mechanical stress to guide and retain light within the photo-active regions of photovoltaics [96]. Devices with such a kind of surface show an obvious improvement in light harvesting efficiency, particularly in the near-infrared region, where light absorption is otherwise minimal, as shown in Figure 10. About a six-fold external quantum efficiency (EQE) improvement could be obtained in the near-infrared region, where the useful range of solar energy conversion is extended by more than 200 nm. The presence of wrinkles and folds can also relieve mechanical stress, effectively increasing the robustness of devices constructed on top of such a surface [97,98]. The devices on a flat surface showed a 90% drop in $J_{SC}$ after 100 cycles, but the device with wrinkled surface exhibited a PCE that was more than 70% its original value.

A design for the top electrode could be more effective for light capture. Rafael *et al.* proposed and implemented an *ad hoc* path for light-harvesting recovery to bring photo-to-charge conversion up to almost 80% that of its opaque counterpart, resulting in a semi-transparent OPV that exhibits 30% visible light transmission and 5.6% PCE, as shown in Figure 11 [99]. The high transmission paved the way for designing and fabricating new types of photovoltaic modules with great potential to be incorporated into buildings as windows, thereby leading to the very good integration of a power generation source in a highly populated urban area.

**Figure 10.** Photon flux diagrams of the optical stacks on flat, wrinkled and composite surfaces: (**a**,**b**) simulations for $\lambda_w$ = 1.8 μm and normal-incidence monochromatic illumination at 488 nm (**a**) and 750 nm (**b**). Red arrows show the net photon flux and blue arrows illustrate large-scale flow. Incident light of a shorter wavelength (488 nm) is efficiently absorbed by the P3HT:PCBM active layer (shown in yellow), so the addition of wrinkles and folds has little effect on the optical path. In contrast, the flow of incident light of longer wavelength (750 nm) is altered significantly, with inplane light trapping leading to a dramatic enhancement in absorption. Cited from [97]. Copyright 2012, Nature.

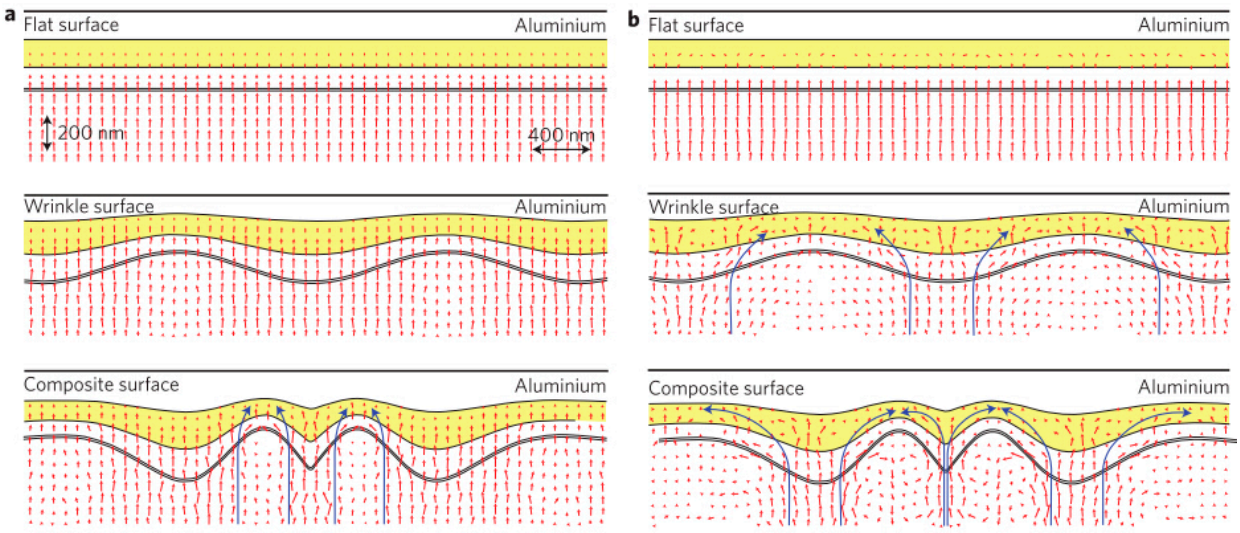

**Figure 11.** Polymer blend and device: (**a**) polythieno(3,4-b)-thiophene-*co*-benzodithiophene (PTB7):(6,6)-phenyl-C71-butyric acid methyl ester ($PC_{70}BM$) extinction coefficient; (**b**) Schematic view of the fabricated photovoltaic cells. Two stripes of ITO were crossed by eight stripes of silver layers defining 9 $mm^2$ cells. The other layers between the electrodes were deposited to cover the entire substrate. A long metal stripe at the back was deposited to contact the ITO. Using a mask, the photonic crystal was grown to cover, as in the schematic, half of the devices. The layer thicknesses given for the photovoltaic part of the structure are the ones used for all semi-transparent devices in the current work. The thicknesses for the photonic-crystal layers correspond to a device for which the current density-voltage curve would be similar to the one shown in (**c**); Layer thicknesses are not fully to scale; (**c**) Current density-voltage curves for the opaque cell (Tk–Ag) (black), semi-transparent cell where top electrode is 10-nm-thick silver layer (Tn–Ag) (red) and the cell incorporating the photonic crystal (PC–Tn–Ag) (green) fabricated with 330 nm ITO. Cited from [99]; Copyright 2013, Nature.

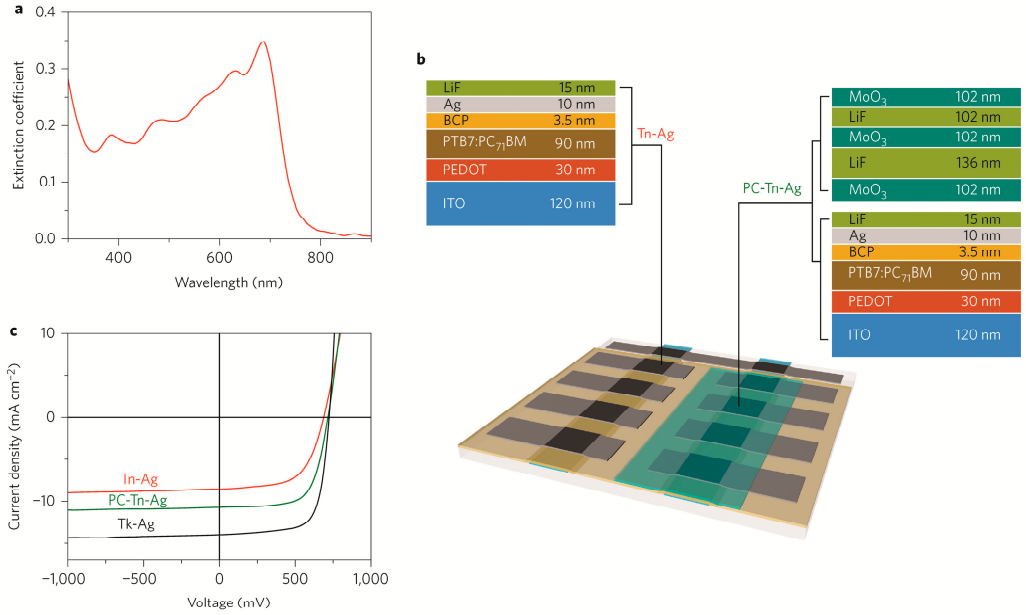


A wire-shaped structure is another attractive type of novel architecture for OPVs, which could be easily sealed with higher safety and scaled up with low cost. A core-sheath structure, where the light could be wave guided into the photoactive layer along the axial direction, has been studied recently [100–102].

Wire-shaped OPV could be divided into two parts: core-sheath architecture based on a single fiber and a twisting architecture from two fibers. In the former type, the P3HT and PCBM were sequentially coated on the optical fiber by a dip-coating process, and the aluminum layer was then deposited on the outer surface by thermal evaporation, as shown in Figure 12. This kind of architecture minimized the reflective and transmissive losses. Moreover, counter electrodes could be replaced by materials with high electron mobility, such as single-walled carbon nanotube (CNT) films [103]. In wire-shaped OPV, the thickness of the active layer is critical to the device performance. The PCE of wire-shaped OPV could be as high as 2.26%–2.31% with a P3HT/PCBM layer of 150–180 nm, which was close to 2.48% for their planar counterparts under identical conditions.

Besides a single fiber electrode, wire-shaped OPVs have also been widely explored by twisting two fiber electrodes [104]. A flexible CNT fiber has been recently developed as one electrode and twisted

with a titanium wire, which was grown with a layer of titanium and coated with photoactive materials, as shown in Figure 13. However, this type of OPVs shows a relatively low efficiency [105].

A recent development in the novel structural designs of OPVs architecture has been presented in the above section. However, there is still a large amount of work on the structure designs of HTL or ETL [106,107], and we cannot present all of them in detail. The reader may find analyses of novel structure designs in other reviews.

**Figure 12.** A wire-shaped OPV based on an optical fiber: (**a**) Schematic illustration; (**b**) Light illumination, propagation and confinement inside the active medium through reflection from Al and the refractive index difference between the layers; and (**c**) Dependence of the current density and efficiency on incident angles with respect to the axis of the optical fiber with a diameter of 1.5 mm. Cited from [100]. Copyright 2007, American Institute of Physics.

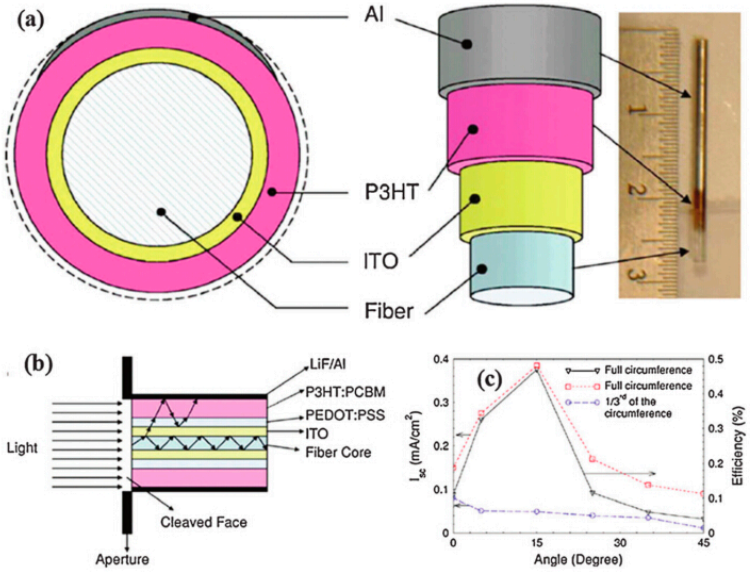


**Figure 13.** A CNT (carbon nanotube) fiber-based OPV: (**a**) schematic illustration; (**b**) *J*–*V* curves, respectively. Cited from [105]. Copyright 2012, The Royal Society of Chemistry.

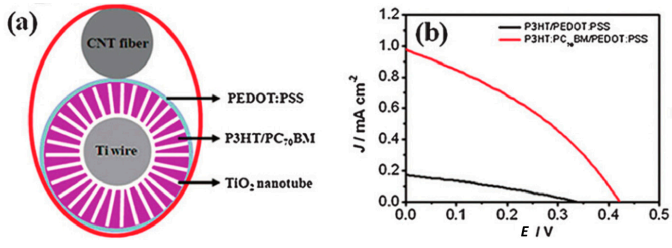


## 4. Approaches for Further Increasing PCE

### *4.1. Thermal Annealing*

Thermal annealing is one of the most widely used post treatments to further increase devices' PCE by controlling the morphology of the active layer [108–112]. Previous research has found that thermal annealing can increase both the crystallinity of P3HT and aggregation of PCBM in a P3HT:PCBM

blend [113,114]. In this case, charge transport could be facilitated, which is mainly ascribed to an increased inplane π–π staking of P3HT for hole transport, and the agglomeration of PCBM provides pathways for electron transport [115,116]. Although the effect of thermal annealing on OPV performance has been demonstrated, more quantitative study of thermal annealing is still necessary.

Previous works on thermal annealing are mainly performed on the analysis of cast and treated devices at optimum temperature and its implication on device physical parameters. In last two years, several novel monitor methods have been introduced in order to further illuminate the mechanism of thermal annealing on the performance of the standard OPV based on P3HT:PCBM BHJ. Oklobia *et al.* investigated the formation of PCBM clusters upon thermal annealing of a P3HT/PCBM BHJ solar cell by using Raman image mapping, which is able to identify the PCBM rich region, as shown in Figure 14 [117]. The diffusion of PCBM molecules to form aggregates was scrupulously manipulated to induce a nano-structure to benefit the device performance by gradually annealing the blend film, from low temperatures through to an optimum temperature. Moreover, Tsoi *et al.* identified the lower fraction of ordered phase (or the higher fraction of disordered phase) in poly(3-hexylselenophene) (P3HS)-based films by means of resonant Raman spectroscopy and wide-angle X-ray scattering [118]. The results denoted that the higher fraction of the disordered phase in P3HS prevents the PCBM in blend films from forming the micrometric size aggregates during thermal annealing, which was different from that of annealed P3HT:PCBM films. Lower fraction, but higher quality of ordered phase in P3HS could benefit P3HS:PCBM photovoltaic performance.

Ng *et al.* used spectroscopic ellipsometry and transmission measurements to investigate the optical properties of P3HT:PCBM before and after thermal annealing [119]. They examined the use of isotropic and anisotropic models with multisample analysis and simultaneous fitting of both transmission and ellipsometry data to describe the annealed P3HT:PCBM blend films. It was found that two different oscillator models resulted in similar *n* and *k* values for isotropic sample models and for the *n* and *k*, corresponding to perpendicular polarization for anisotropic sample models, whereas there were differences in parallel polarization optical functions, as shown Figure 15.

**Figure 14.** Raman spectra recorded for a thermally annealed thin film (P3HT:PCBM, 1:1). This was taken from two points: (1) at a point containing PCBM aggregates, showing a weak Raman signal for P3HT (**a**); and (2) at a uniform region, showing strong Raman signal for P3HT (**b**), indicating a P3HT-rich region. Cited from [117]. Copyright 2013, Elsevier.

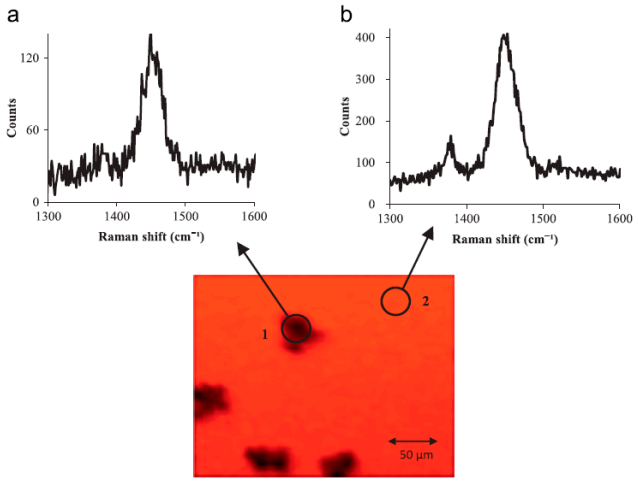

**Figure 15.** Obtained *n* and *k* values for perpendicular and parallel polarizations, respectively. Cited from [119]. Copyright 2013, America Chemistry Society.

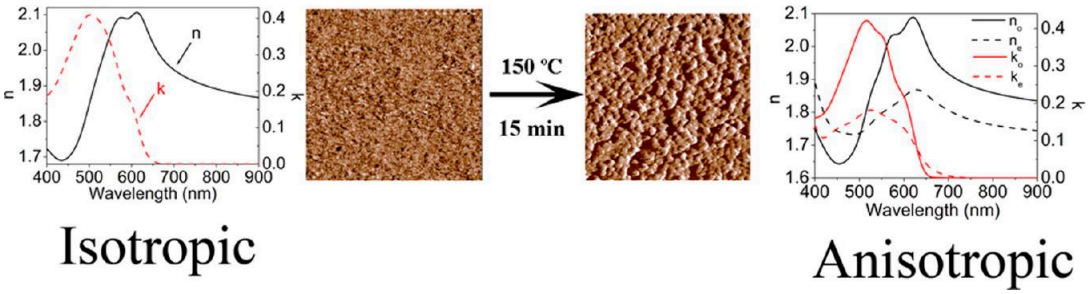


Furthermore, Zhao *et al.* introduced optical absorption and photoexcitation-assisted capacitance–voltage (*C*–*V*) measurements to study the internal electrical polarization effect in the standard P3HT:PCBM solar cells [120]. Treated by thermal annealing, the light absorption of active layer could be observed, which was ascribed to the morphological development. Furthermore, the enhancement in absorption coefficient indicates stronger electrical polarization in the P3HT:PCBM films, leading to an enhancement on the generation of charge carrier at the D:A interface and the transport of generated charge carriers to the respective electrode interface in the P3HT:PCBM device. Shih *et al.* monitored *in situ* the change of P3HT:PCBM during thermal annealing [121]. They found that an annealing temperature higher than the glass transition temperature of P3HT (127 °C) is critical to the improvement of $V_{OC}$. The *in situ* monitoring of electron/hole transport disclosed the variation of $J_{SC}$ and was a thermally activated process.

In spite of the optical measurements, morphology descriptions are also important to illuminate the mechanism of thermal annealing. Wodo *et al.* presented a graph-based framework to efficiently compute a broad suite of physically morphology descriptors [122]. Two large sets of morphologies with the blend weight ratios of 1:1 and 1:0.82 (A:D) have been employed to study thermal annealing, as shown in Figure 16. Thermal annealing could increase the feature size and coarsening of the morphology. It revealed that the coarsening of the morphology could improve the quality paths, as well as the total fraction of useful domains. At a certain point, the exciton dissociation becomes the bottleneck during annealing and cannot be compensated by the improving charge transport. However, the result of Wodo's work showed that during thermal annealing, charge transport is the initial bottleneck rather than exciton dissociation.

A combination of energy filtered transmission electron microscopy (EFTEM) and thermally stimulated current was used to investigate the effect of thermal annealing on the OPV performance, as shown in Figure 17 [123]. Thermal annealing for 10 min at 130 °C resulted in a better reordering of P3HT and PCBM into better domains and higher density of trap states in the P3HT phase compared to the as-cast OPV. Annealing of P3HT:PCBM solar cells had a beneficial impact not only on the local molecular order, but in particular on providing percolation paths for charge carriers.

Nieuwendaal *et al.* employed $^{1}$H spin diffusion nuclear magnetic resonance ($^{1}$H NMR) spectroscopy to measure the domain size and compositional heterogeneities in P3HT/PCBM BHJ, as shown in Figure 18 [124]. They showed that the domains with a size of tens of nanometers and greater spatial homogeneity are favorable for a higher PCE. Furthermore, thermal annealing is less optimal than slow

solvent casting as a means to achieve the desired degree of phase separation in polymer-fullerene BHJ films.

**Figure 16.** Representative two-phase morphology evolution obtained via numerical simulation of thermal annealing for two blend ratios (1:1 and 1:0.82) from early stages (first row) until the final time (consecutive rows). Efficiencies as a function of annealing time *t* (dimensionless) for two different blend ratios. Plots show estimates of efficiencies for blend ratios 1:1 and 1:0.82. Cited from [122]. Copyright 2012, Elsevier.

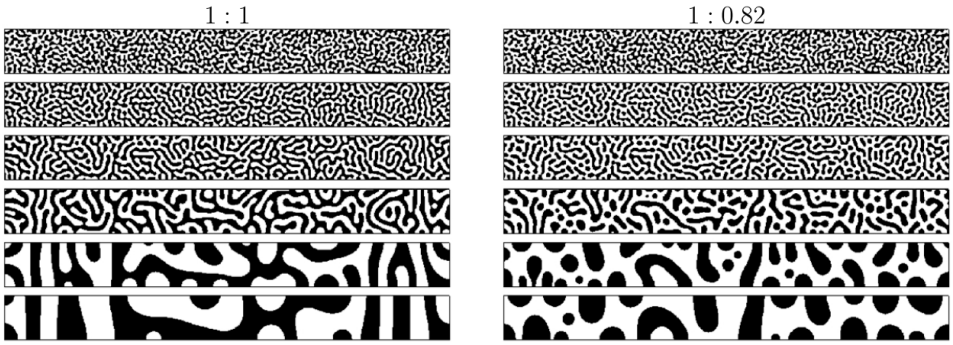


**Figure 17.** TEM (transmission electron microscope) and energy filtere TEM- element specific imaging (ESI) micrographs from a cross-section of the solar cell: (**a**,**b**) bright-field-TEM images of the pristine and the annealed device; (**c**,**d**) ESI images of the solar cell before and after annealing for 10 min at 130 °C. The color scale displays the varying sulfur concentrations throughout the photoactive layer. The cross-sections were prepared by microtome cutting, which induces a high mechanical stress in the layers and can cause layer delamination. Because of this delamination, the top electrode is missing in the image of the pristine solar cell cross-section; (**e**,**f**) The profile analysis along the white arrows (in Panels **c** and **d**) revealed a more pronounced relative sulfur distribution for the annealed sample. Cited from [123]. Copyright 2013, America Chemical Society.

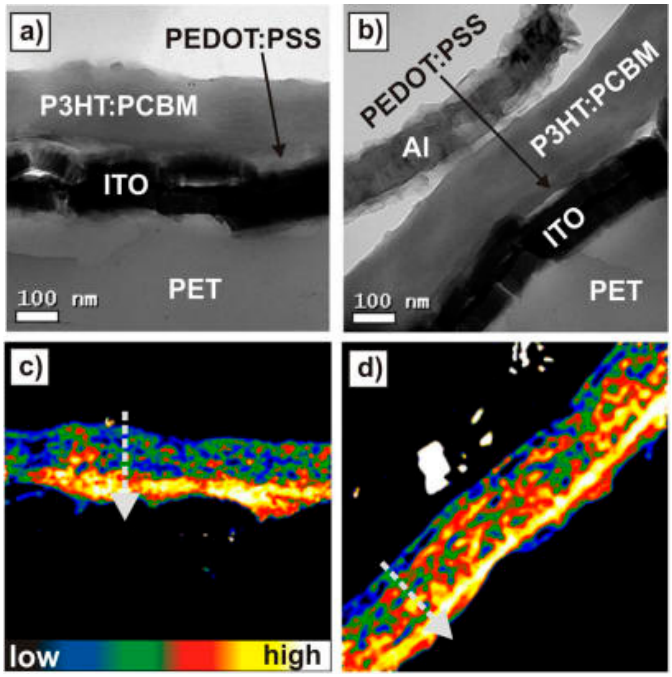

**Figure 17.** *Cont.*

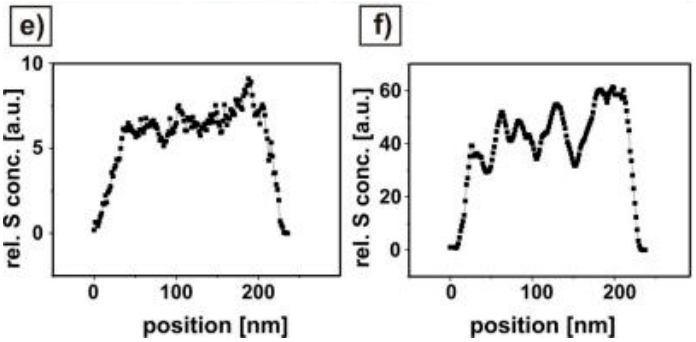


**Figure 18.** $^{1}$H NMR spectra of P3HT-PCBM: (**a**) combined rotation and multiple pulse spectroscopy (CRAMPS) spectrum of the physical mixture (50:50 by mass); (**b**) CRAMPS spectra of the neat components (PCBM is inverted) demonstrate the component breakdown of (**c**) the spin diffusion spectrum of the physical mixture ($t_m$ = 2 ms); (**d**) CRAMPS spectrum of the slow-spin unannealed thin film blend; (**e**) the spin diffusion spectrum of the physical mixture ($t_m$ = 2 ms); and (**f**)–(**i**) spin diffusion spectra of the slow-spin unannealed thin film blend for $t_m$ = 2 ms (**f**), 30 ms (**g**), 60 ms (**h**) and 240 ms (**i**). Cited from [124]. Copyright 2012, Wiley.

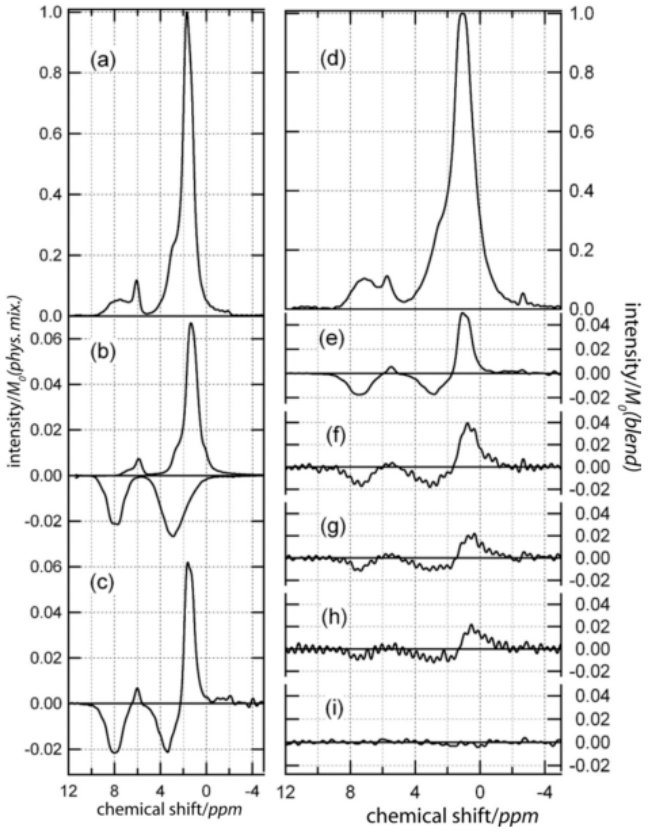


Besides the above investigation, many groups paid attention to applying thermal annealing to increase the PCE of OPV in other donor-PCBM systems. Keivanidis *et al.* found that thermal annealing of the PIF8BT:PDI at 90 °C has a positive impact on the photocurrent generation efficiency and yields a corresponding increase in PL quenching [125]. It was also reported that thermal annealing could change

the packing of poly[2,6-(4,4-bis(2-ethylhexyl)-4*H*-cyclopenta(2,1-b;3,4-b')-dithiophene)-*alt*-4,7-(2,1,3-benzothiadiazole)] (PCPDTBT) [126]. However, thermal annealing might cause some detriment to device performance. Street *et al.* demonstrated that thermal annealing could induce both nanostructure and electronic changes and broaden the exponential band tails and then increase the recombination rate by investigating the effect of thermal annealing on the performance of poly[(9-(1-octylnonyl)-9*H*-carbazole-2,7-diyl)-2,5-thiophenediyl-2,1,3-benzothiadiazole-4,7-diyl-2,5-thiophenediyl)] PCDTBT:PCBM OPV [127]. It was also shown that the glass transition temperature of the blend reduces upon annealing; an observation consistent with the disruption of π–π stacking between PCDTBT molecules. Reduced π–π stacking is correlated with reduced hole-mobility in thermally annealed films [128].

### *4.2. Polar Solvent Annealing*

Although thermal annealing could benefit the charge transport and separation efficiency in the D/A interface by facilitating the interdiffusion of the donor to PCMB, the limitation of thermal annealing is also obvious. Large-scale phase separation and the formation of structures could be detrimental to the device performance [129]. Extended thermal annealing has been shown to create a large aggregation of PCBM with a scale of tens to hundreds of micrometers, which exceeds the diffusion length of separated excitons [130]. This phenomenon can also result in the coarsening of nanoscale phase segregation, leading to unfavorable charge recombination and lower PCE [131]. Moreover, the high temperature of thermal annealing could probably impede the function of conjugated polymer and flexible substrate [132]. Furthermore, thermal annealing provides a rapid process for structural change, but crystallization and phase separation in the active layer could not be examined separately [133].

To achieve high device performance without damaging the polymers, the precise morphology control of the active layer is necessary. To this end, solvent vapor annealing (SVA) has been explored in recent years [134–139]. SVA is a versatile method, where a thin film is exposed to an atmosphere of solvent vapor diffusing into the deposited layer, the extent of which is dependent on and thus controllable by exposure time [134].

Zhang *et al.* elucidated the primary dynamics of exciton and charge photogeneration in SVA-treated OPV based on P3HT/PCBM BHJ by incorporating spectroelectrochemistry and time-resolved spectroscopy [136]. It was found that the SVA could promote the formation of P3HT nanocrystallites via self-organization. For the SVA-treated active layer, the red-edge excitation induced both instantaneous and delayed polaron formation, and blue-edge excitation induced prompt formation of polaron absorption in 830–1000 nm. The SVA blend films exhibited a dimension of exciton delocalization of ~7.6 nm and 6.6 nm under excitation wavelengths of 620 and 460 nm, respectively. SVA could avoid the random P3HT phases and reduce the disordered or amorphous polymer/PCBM aggregate, which were considered to be the polaron traps and carrier blocks, resulting in the polaron recombination and the decrease of free charge mobilities.

In addition, mesoscopic PCBM crystallites in SVA-treated OPV were studied by many groups. Bull *et al.* examined the role of PCBM crystallites by employing the scanning light beam-induced current (LBIC) technique, as shown in Figure 19 [137]. The results showed that SVA could lead to the formation of mesoscopic PCBM crystallites, ripening of electron-transporting domains, as well as the formation of a copolymer-rich overlay. However, the large crystallites of PCBM did not directly

improve the PCE; they were associated with the surrounding regions of increased light absorption and improved photocurrent. Similar results were also found in the study of Nam *et al.* [138]. It was revealed that the solubility of alcohols is a key factor for controlling the morphologies, which determines the size of PCBM crystallites. In addition, Verploegen *et al.* observed the morphology of a P3HT/PCBM blend in real time by using grazing incidence X-ray scattering (GIXS) [139]. The SVA with chloroform and tetrahydrofuran (THF) can lead to smaller phase segregated domains (~52 Å and 62 Å, respectively) than thermal annealing at 130 °C (>130 Å). SVA results in the π–π stacking direction being predominately perpendicular to the substrate, which is more favorable for charge transport than the predominately parallel π–π stacking direction, as observed with thermal annealing. Moreover, Huang *et al.* reported the effect of dichlorobenzene (DCB) SVA on the performance of spray-coated OPV [140]. Compared to thermal annealing, DCB SVA shows a 20% increase in device PCE via ordered P3HT chains staking and PCBM cluster growing. A PCE of 3.61% could be obtained by combining the subsequent thermal annealing.

**Figure 19.** (**a**) Light beam-induced current (LBIC) map of 30-min solvent vapor annealing (SVA) 1:5 poly(4,7-bis(3-dodecylthiophen-2-yl)thieno(3,4-b)pyrazine-*alt*-9,9-dioctyl-2,7-fluorene) (BTTP-F)/PCBM film with a large PCBM crystallite. The PCBM crystallite does not generate large photocurrents, but a region surrounding the crystallite is enhanced; (**b**) *I–V* characteristics corresponding to locations on Panels **a**,**c**. The crystallite (**A**) produces the smallest power followed by the unannealed blend (**D**,**E**), but the enhanced region in the annealed blend (**B**) and the matrix (**C**) produce the greatest power; (**c**) LBIC map of the unannealed blend showing uniform photocurrent generation. Cited from [136]. Copyright 2012, America Chemical Society.

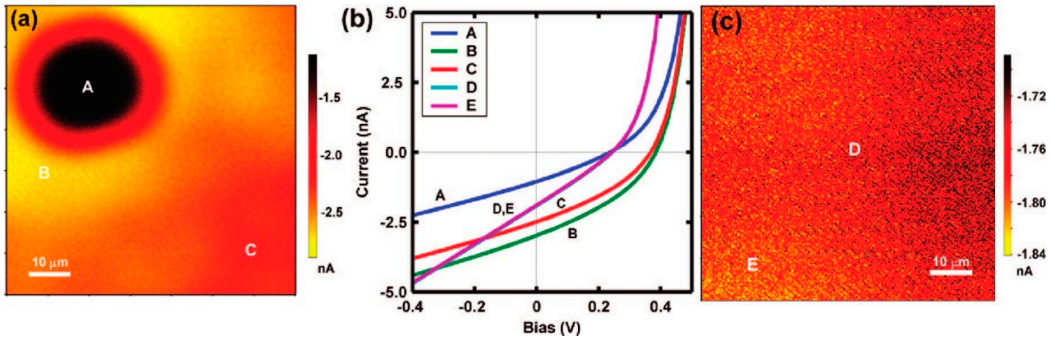


Furthermore, several modification approaches based on solvents have also been reported with the capability of a significant enhancement of device performance. Li *et al.* employed solvent-soaking treatment to control the morphology of OPV active layer, resulting in the increase of PCE from 1.45% to 3.23% [141]. $CH_3OH/CS_2$ mixed solvent was incorporated to immerse the P3HT/PCBM blends, leading to the interpenetrating network of P3HT crystallites and PCBM nanoscale aggregates, as well as vertical phase separation of P3HT/PCBM. Moreover, solvent simply spin cast on the active layer could also benefit the OPV performance. Jeon *et al.* employed non-solvent swelling to treat the OPV [142]. Combining with the post-annealing treatment, a PCE of device from 1.58% to 3.01% has been obtained, resulting from: (1) a red shift of UV–Vis absorption maximum peak; (2) an increase in the penetration depth of the Al layer on the active layer; and (3) surface topology changes of the active layer. Zhou *et al.* used methanol on the top of a PTB7/PCBM surface to improve the PCE of devices by passivating the

surface traps and increasing the surface charge density [143]. Faster decay kinetics after methanol treatment indicated a faster extraction of the mobile carrier, which was detected by the internal field-dependent transient photoconductivity measurement. In addition, Lee *et al.* reported that using 2-methoxyethanol and ethanolamine co-solvent to modify the ZnO interface in OPV based on PTB7/PCBM BHJ could lead to increased electron mobility, suppressed bimolecular recombination and minimized contact resistance [144].

The overall device characteristics of OPVs with different polar solvent treatments were improved with varied successes, which are summarized in Table 1.

**Table 1.** Summary of device characteristics of OPVs with different polar solvent treatments. FF, fill factor; PCE, power conversion efficiency.

| Solvents | Methods | Active Layer | $V_{OC}$ (V) | $J_{SC}$ (mA/cm$^2$) | FF (1) | PCE (%) | Ref. |
|---|---|---|---|---|---|---|---|
| Methanol (ME) | Direct exposure | P3HT/$PC_{60}BM$ | 0.63 | 9.40 | 0.52 | 2.9 | [138] |
| Ethanol | Direct exposure | P3HT/$PC_{60}BM$ | 0.64 | 10.20 | 0.56 | 3.25 | [138] |
| Propanol | Direct exposure | P3HT/$PC_{60}BM$ | 0.64 | 9.26 | 0.47 | 2.7 | [138] |
| Butanol | Direct exposure | P3HT/$PC_{60}BM$ | 0.64 | 9.27 | 0.45 | 2.76 | [138] |
| Methanol | Solvent annealing | PTB7/$PC_{70}BM$ | 0.72 | 14.69 | 0.73 | 7.72 | [144] |
| Ethanol (EA) | Solvent annealing | PTB7/$PC_{70}BM$ | 0.72 | 14.75 | 0.72 | 7.65 | [144] |
| 2-ME | Solvent annealing | PTB7/$PC_{70}BM$ | 0.71 | 14.45 | 0.71 | 7.28 | [144] |
| 2-ME + EA (1%) | Solvent annealing | PTB7/$PC_{70}BM$ | 0.71 | 16.76 | 0.73 | 8.69 | [144] |
| Methanol | Solvent annealing | PTB7/$PC_{70}BM$ (Al cathode) | 0.75 | 13.92 | 0.68 | 7.20 | [143] |
| Methanol | Solvent annealing | PTB7/$PC_{70}BM$ (Ca/Al cathodes) | 0.76 | 15.46 | 0.68 | 7.94 | [143] |
| Chlorobenzene (CB) | Solvent annealing | PBDTTPD/$PC_{70}BM$ | 0.88 | 9.11 | 0.61 | 4.92 | [145] |
| DCB | Solvent annealing | PBDTTPD/$PC_{70}BM$ | 0.89 | 10.52 | 0.53 | 4.99 | [145] |
| DCB | Solvent annealing | *p*-phenylenevinylene copolymer/$PC_{70}BM$ | 0.81 | 6.32 | 0.55 | 2.80 | [146] |
| Chloroform (CF) | SVA | PCDTBT/$PC_{70}BM$ | 0.87 | 15.65 | 0.52 | 7.03 | [147] |

PBDTTPD: poly(benzo(1,2-b:4,5-b')-dithiophene−thieno(3,4-c)pyrrole-4,6-dione).

### *4.3. Additive*

In addition to annealing treatment, recently the use of additives has attracted extraordinary attention over the annealing process because of its ease of implementation and effectiveness in enhancing the device performance, which does not require an additional fabrication step [148]. Additives were firstly found to be effective in P3HT/PCBM-based devices and then to be extended to the low-bandgap polymer-based devices, e.g., PCPDTBT and poly(4,8-bis(5-(2-ethylhexyl)thiophen-2-yl)benzo[1,2-b:4,5-b'] dithiophene-2,6-diyl) (PBDTBDD ) [149]. Two general guidelines for additive design are as follows: (1) the boiling point must be significantly higher than that of the processing solvent to maximize the interaction time between the additive and the active layer components during thin film formation; and (2) one active layer component must be significantly more soluble in the additive than other components [150]. Recent promising additives fulfilling these guidelines have been incorporated in enhancing the OPV performance [151,152].

For BHJ systems containing donor polymers, such as PTB7, PCPDTBT and others, 1,8-diiodooctane (DIO) affords the highest PCE enhancement observed to date [153–156]. Recently, several groups have employed advanced characterization methods to investigate the changes in the active layer. Lou *et al.* used small-angle X-ray scattering techniques to analyze the effects of DIO on the aggregation of PTB7/PCBM-based OPV [157]. The DIO added to a CB could completely dissolve the $PC_{70}BM$ aggregates, promoting the formation of smaller domains and greater donor-acceptor interpenetration within the active layer. This may be attributed to the opposite charge of the iodine atom and $PC_{70}BM$ shares, leading to the strong interaction with each other and the enhanced solubility of $PC_{70}BM$ in the presence of DIO. Furthermore, grazing incidence X-ray diffraction (GIXD), small-angle neutron scattering and resonant soft X-ray scattering were carried out to determine the crystallinity and phase separation of the resultant PCPDTBT/PCBM thin films processed with or without additives [158]. The GIXD results presented that the primary function of an additive is to act as a nonsolvent for the PCPDTBT and a good solvent for the PCBM, wherein the CB, a good solvent for both PCPDTBT and PCBM, evaporates; the mixed solvent becomes poorer for the PCPDTBT, whereas the PCBM remains solubilized. With further evaporation of CB, the solvent quality for the PCPDTBT decreases and the PCPDTBT aggregates and crystallizes into fibrils, whereas the PCBM remains dispersed. During the final stage of solvent evaporation and as the additive evaporates, the PCBM and remaining non-crystalline PCPDTBT aggregations fill the interfibrillar regions, as shown in Figure 20.

In addition to conventional donor materials, the effect of DIO has also been demonstrated in the novel donor-acceptor BHJ. Ye *et al.* utilized 3 vol% DIO to optimize the OPV based on PBDTBDD: bis adduct of phenyl-C61-butyric acid methyl ester (Bis-PCBM) (1:1 *w*/*w*), resulting in a high PCE of 6.07% with a relatively high $V_{OC}$ of 1.00 V, compared to 4.55% for the OPV without DIO [159]. Moreover, Dou *et al.* applied DIO to optimize the morphology of active layer based on novel polymers, including PBDTT-DPP, PBDTPDPP, PBDTT-FDPP and PBDTP-FDPP [160]. Furthermore, Do *et al.* demonstrated that the DIO was related to the different response to the novel materials [161].

Similar to DIO, adding a small volume of 1,8-octanedithiol (ODT), 1,8-dichlorooctane (DCO) and 1-chloronaphthalene (CN) in the active layer has been demonstrated to improve the PCE of OPV significantly [162–164]. Etzold *et al.* used solid-state nuclear magnetic resonance (NMR) spectroscopy to study in detail the effect of ODT on the morphology and excited state dynamics in PCPDTBT:PCBM

BHJ [162]. ODT could significantly reduce the total internal quantum efficiency loss due to the geminate recombination by about 30% and facilitate more free charge generation. Aïch *et al.* combined two conventional additives of DIO and CN to utilize as the co-additives in ortho-dichlorobenzene and CB solution to tune the donor and acceptor domains in PBDTTPD/PCBM BHJ [165]. In the co-additive system, CN enhances the solubility of the polymer and suppresses the formation of large polymer domains, while DIO acts as a PCBM crystallization controller, resulting in performance enhancement from PCE = 3.2% of 3% DIO only and PCE = 4.7% of 4% CN only to PCE = 7.1% of co-additive of 4% CN and 1% DIO. Furthermore, Chang *et al.* verified that PCBM crystallization is favored over P3HT crystallization in DIO/CB and CN/CB BHJ films [166]. In particular, the OPVs based on addition of CB, nitrobenzene (NB), DIO and CN all remained stable over at least 300 h.

**Figure 20.** Morphology for PCPDTBT/PCBM thin films processed without additives (**a**) or with additives (**b**). Cited from [158]. Copyright 2012, Wiley.

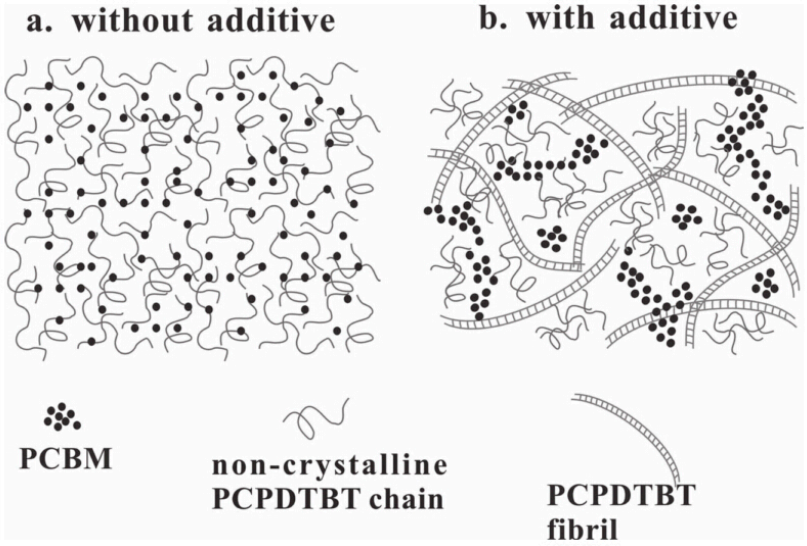


The squaraine (SQ) donor is another type of additive, which also shows great potential in being using as the donor in OPVs. Huang *et al.* incorporated the squaraine dye in P3HT/PCBM blends to obtain a 38% increase in PCE [167]. It was found that the squaraine additive could benefit the exciton migration, which was detected by femtosecond spectroscopy. Squaraine additive could also improve the near-infrared absorption of the active layer [168].

Despite the conventional additive, several novel additives were also introduced to improve the performance of OPV in recent years. Lobez *et al.* presented a new class of additives based on regioregular poly(thiophene)s [169], where the side chains of this polymer have been functionalized at the termini in every other thiophene unit, leading to the enhancement in $J_{SC}$ from 9.32 to 12.2 mA/cm$^2$. 4-Bromoanisole (BrAni) is another effective additive for P3HT blends [170]. One percent BrAni could result in the PCE of OPV based on P3HT/PCBM BHJ being improved from 3.32% to 4.15% [171]. Moreover, adding 1:250 of 2,3,5,6-tetrafuloro-7,7,8,8-tetracyanoquinodimethane (F4-TCNQ) on the active layers of PCDTBT:$PC_{70}BM$ could improve the PCE from 6.41% to 7.94%, which was mainly ascribed to the enhancement of $J_{SC}$ from 11.0 to 14.0 mA/cm$^2$ [172]. Furthermore, 1.5% N-doped carbon nanotube was found to be an effective additive in PTB7:PCBM BHJ, resulting in an enhanced PCE from

7.3% to 8.6% [173]. In addition, 2,3-bis(5-bromothiophene-2-yl)acrylonitrile (DTDBAL) was synthesized by Chen *et al.* to improve the charge transport and exciton dissociation in the P3HT/PCBM system, and a 36% increase in PCE has been observed [174]. Besides, 13% polyvinylcarbazole (PVK) was introduced in P3HT:$IC_{60}BA$ BHJ to significantly increase the $V_{OC}$ from 0.56 to 0.78 V, which was attributed to the modified interpenetrating networks of P3HT:$IC_{60}BA$ [175].

Additives have been demonstrated to significantly improve OPV performance, and recent additives applied in OPVs are listed in Table 2. Despite the widely used DIO, a large amount of materials have the potential of being applied in these systems. An additive with near-infrared absorption and high charge mobility would be very promising. Still, these are a lot of problems to be addressed, including the accurate characterization of additive in the active layer for the understanding of the mechanism of the D–A-additive system, the detailed regulation of additive concentration and the decrease of the charge recombination rate during the charge transfer process at the D/additive or A/additive interface.

**Table 2.** Summary of device characteristics of OPVs based on various additives.

| Additives | Vol (%) | Solvent | Active Layer | $V_{OC}$ (V) | $J_{SC}$ (mA/cm$^2$) | FF (1) | PCE (%) | Ref. |
|---|---|---|---|---|---|---|---|---|
| DIO | 3 | CF | BDT-DPP/$PC_{70}BM$ | 0.76 | 8.49 | 0.60 | 3.88 | [176] |
| DIO | 7 | ODCB | BDT-DPP/$PC_{70}BM$ | 0.72 | 11.86 | 0.61 | 5.29 | [176] |
| DIO | 2.5 | - | PCPDTBT/$PC_{70}BM$ | 0.62 | 14.90 | 0.50 | 4.62 | [158] |
| DIO | 3 | - | PBDTBDD/Bis-PCBM | 1.00 | 10.02 | 0.61 | 6.07 | [159] |
| DIO | 3 | - | PBDTFBZS/$PC_{70}BM$ | 0.88 | 12.03 | 0.71 | 7.74 | [177] |
| DIO | 3 | ODCB | PBDTTPD/$PC_{70}BM$ | 0.87 | 6.6 | 0.55 | 3.2 | [165] |
| CN | 4 | ODCB | PBDTTPD/$PC_{70}BM$ | 0.85 | 9.4 | 0.59 | 4.7 | [165] |
| CN + DIO | 10 + 1 | ODCB | PBDTTPD/$PC_{70}BM$ | 0.87 | 11.0 | 0.67 | 6.4 | [165] |
| CN + DIO | 4 + 1 | CB | PBDTTPD/$PC_{70}BM$ | 0.93 | 10.89 | 0.70 | 7.1 | [165] |
| MeN + DIO | 2 + 3 | Xylenes | PDTSTPD/$PC_{70}BM$ | 0.89 | 11.7 | 0.60 | 6.2 | [178] |
| ODT | 2.5 | - | PCPDTBT/$PC_{70}BM$ | 0.61 | 14.39 | 0.44 | 3.87 | [158] |
| DCO | 2.5 | - | PCPDTBT/$PC_{70}BM$ | 0.63 | 11.80 | 0.46 | 3.45 | [158] |
| BrAni | 1 | - | P3HT/$PC_{60}BM$ | 0.63 | 11.16 | 0.59 | 4.15 | [171] |
| BrAni | 2 | - | N(Ph-2T-DCN-Et)$_3$/$PC_{70}BM$ | 0.96 | 7.81 | 0.50 | 3.60 | [170] |
| P6 | 0.25 | - | P3HT/$PC_{60}BM$ | 0.60 | 12.2 | 0.53 | 3.78 | [169] |
| F4-TCNQ | 0.004 | - | PCDTBT/$PC_{70}BM$ | 0.90 | 14.0 | 0.63 | 7.94 | [172] |
| N-MCNTs | 1.5 | - | PTB7/$PC_{70}BM$ | 0.7 | 17.4 | 0.69 | 8.41 | [173] |
| SQ | 1 | - | P3HT/$PC_{60}BM$ | 0.60 | 11.6 | 0.65 | 4.51 | [167] |
| DPSQ | 5 | - | P3HT/$PC_{60}BM$ | 0.61 | 8.9 | 0.68 | 3.65 | [168] |
| Me-naph | 2 | Toluene | PIDT-phanQ/$PC_{70}BM$ | 0.87 | 10.8 | 0.65 | 6.1 | [179] |
| Me-naph | 2 | *o*-Xylene | PIDT-phanQ/$PC_{70}BM$ | 0.86 | 10.5 | 0.63 | 5.7 | [179] |
| DTDBAL | 0.05 | - | P3HT/$PC_{60}BM$ | 0.66 | 10.58 | 0.52 | 3.60 | [174] |
| DPP-CN | 8 | CN/THF | P3HT/$PC_{60}BM$ | 0.66 | 12.29 | 0.58 | 4.70 | [180] |
| PVK | 13 | - | P3HT/$IC_{60}BA$ | 0.78 | 9.1 | 0.50 | 3.5 | [175] |
| PCBTTE | 5 | - | P3HT/$PC_{60}BM$ | 0.61 | 11.06 | 0.65 | 4.37 | [181] |

MeN, methyl naphthalene; BDT-DPP, benzodithiophene-diketopyrrolopyrrole; N(Ph-2T-DCN-Et)$_3$, tris{4-[5"-(1,1-dicyanobut-1-en-2-yl)-2,2'-bithiophen-5-yl]phenyl}amine; DPSQ, diphenyl-functionalized squaraine; N-MCNTs, N-doped multiwall carbon nanotubes; Me-naph, 1-methylnaphthalene; DPP-CN, diketopyrrolopyrrole-cyanovinylene-4-nitrophenyl; PCBTTE, [6,6]-phenyl-C61-butyric acid 2-(2′,2′:5′,2′-terthiophene-5′-yl)ethyl ester.

## 5. Conclusions and Outlook

Recent developments in OPVs have shown that, assisted with the further illustration of the key photophysical process in OPV, the design of a novel structure and the application of efficient modification, the performance of OPVs can be significantly improved. It is believed that the maximum PCE of OPVs must rise above 15% in the laboratory before they can be practically useful, which has been realized by the perovskite OPVs and is getting close in polymeric OPVs. For a reachable PCE limit of 22%–27% [182], further work should be focused on the descriptions below:

(i) It is part of a trend to apply an apparatus with a capability of capturing the motion trail of charge carriers at the femtosecond level for the characterization of the photophysical process in OPV. With the advance in characterization techniques, the mechanism of charge transfer could be more clearly understood, leading to the better design and synthesis of organic functional materials with low-bandgap and strong near-infrared absorption;

(ii) The design of a novel device architecture is an efficient way for improving the PCE. To break the limit of conventional thin film BHJ, there have been several new architectures, e.g., wrinkled surface, wire-shape OPV and nanostructured OPV, to be realized to trap more incident light and to pave the way for more efficient charge transfer. The future work in this area should be focused on designing large-scale compatible and low-cost processable architecture;

(iii) Post modification is a convenient method to benefit the device performance directly. The general annealing, including solvent annealing and thermal annealing, is also effective with respect to the new synthesized materials. However, the mechanism of these conventional annealing process is still unclear. With the development of characterization methods, much effort should be made on the illustration of these modifications for more precise control. Moreover, there is a large amount of novel modification that can be incorporated to make a contribution toward high device performance, e.g., soaking method, doping additives and inversing methods.

In this review, we would like to bring some insights to the readers via expatiating the recent advantages in OPV. This current knowledge is far from complete. However, rapid progress is being made, without any doubt with respect to the writing of this review. This review demonstrates not only that there is a lot more work to be performed, but also that the promise of OPVs, which are carving avenues towards future environmentally-benign and sustainable power sources, is greater than ever.

## Acknowledgments

This work is supported by the National Science Foundation of China (Grant No. 61177032), the Fundamental Research Funds for the Central Universities (Grant No. ZYGX2010Z004), and the Foudation of Innovation Groups of NSFC (No. 61421002).

## Author Contributions

Junsheng Yu is the supervisor of Zheng and Huang and the corresponding author of this work and carried out the part 1. Jiang Huang mainly made contribution on part 2. Yifan Zheng mainly focused on writing the part 3 and 4. All authors read and approved the final manuscript.

## Conflicts of Interest

The authors declare no conflict of interest.

## References


1. Gan, Q.; Bartoli, F.J.; Kafafi, Z.H. Plasmonic-enhanced organic photovoltaics: Breaking the 10% efficiency barrier. *Adv. Mater.* **2013**, *25*, 2385–2396.
2. Green, M.A.; Emery, K.; Hishikawa, Y.; Warta, W.; Dunlop, E.D. Solar cell efficiency tables. *Prog. Photovolt. Res. Appl.* **2012**, *20*, 12–20.
3. Green, M.A. Recent developments in photovoltaic. *Sol. Energy* **2004**, *76*, 3–8.
4. Bauhuis, G.J.; Mulder, P.; Haverkamp, E.J.; Huijben, J.C.C.M.; Schermer, J.J. 26.1% thin-film GaAs solar cell using epitaxial lift-offs. *Sol. Energ. Mater. Sol. Cells* **2009**, *93*, 1488–1491.
5. Contreras, M.A.; Egaas, B.; Ramanathan, K.; Hiltner, J.; Swartzlander, A.; Hasoon, F.; Noufi, R. Progress toward 20% efficiency in Cu(In,Ga)$Se_2$ polycrystalline thin-film solar cells. *Prog. Photovoltaics* **1999**, *7*, 311–316.
6. Romeo, A.; Terheggen, A.; Abou-Ras, D.; Batzner, D.L.; Haug, F.J.; Kalin, M.; Rudmann, D.; Tiwari, A.N. Development of thin-film Cu(In,Ga)$Se_2$ and CdTe solar cells. *Prog. Photovoltaics* **2004**, *12*, 93–111.
7. Solar PV Manufacturing Cost Analysis. Available online: http://www.nrel.gov/analysis/key_activities_jobs_pv_mfg_cost.html (accessed on 10 October 2011).
8. Dou, L.; You, J.; Hong, Z.; Xu, Z.; Li, G.; Street, R.A.; Yang, Y. A decade of organic/polymeric photovoltaic research. *Adv. Mater.* **2013**, *25*, 6642–6671.
9. Zhou, N.J.; Buchholz, D.B.; Zhu, G.; Yu, X.G.; Lin, H.; Facchetti, A.; Marks, T.J.; Chang, R.P.H. Ultraflexible polymer solar cells using amorphous zinc-indium-tin oxide transparent electrodes. *Adv. Mater.* **2014**, *26*, 1098–1104.
10. Zhao, J.; Liu, L.; Wu, J.; Yu, J.S. Spectral variation of solution-processed blue bis[(4,6-difluorophenyl)-pyridinato-N,$C^{2'}$] (picolinate) iridium(III) phosphor. *Dyes Pigments* **2014**, *102*, 234–241.
11. Huang, J.; Wang, H.Y.; Qi, Y.G.; Yu, J.S. Influence of bias voltage and temperature on charge transfer states in organic photovoltaic and electroluminescent integrated device. *Appl. Phys. Lett.* **2011**, *104*, 203301.
12. Li, G.; Zhu, R.; Yang, Y. Polymer solar cells. *Nat. Photonics* **2012**, *6*, 153–161.
13. You, J.; Dou, L.; Yoshimura, K.; Kato, T.; Ohya, K.; Moriarty, T.; Emery, K.; Chen, C.; Gao, J.; Li, G.; *et al.* A polymer tandem solar cell with 10.6% power conversion efficiency. *Nat. Commun.* **2013**, *4*, 1446.
14. Clarke, T.M.; Durrant, J.R. Charge photogeneration in organic solar cells. *Chem. Rev.* **2010**, *110*, 6736–6767.
15. Janssen, R.A.J.; Nelson, J. Factors limiting device efficiency in organic photovoltaics. *Adv. Mater.* **2013**, *25*, 1847–1858.

16. Bakulin, A.A.; Martyanov, D.S.; Paraschuk, D.Y.; Pshenichnikov, M.S.; van Loosdrecht, P.H.M.J. Ultrafast charge photogeneration dynamics in ground-state charge-transfer complexes based on conjugated polymers. *J. Phys. Chem. B* **2008**, *112*, 13730.
17. Zhou, N.J.; Lin, H.; Lou, S.J.; Yu, X.G.; Guo, P.J.; Manley, E.F.; Loser, S.; Hartnett, P.; Huang, H.; Wasielewski, M.R.; *et al.* Morphology-performance relationships in high-efficiency all-polymer solar cells. *Adv. Energy Mater.* **2014**, doi:10.1002/aenm.201300785.
18. Guo, X.G.; Zhou, N.J.; Lou, S.J.; Smith, J.; Tice, D.B.; Hennek, J.W.; Ortiz, R.P.; Navarrete, J.T.L.; Li, S.Y.; Strzalka, J. Polymer solar cells with enhanced fill factors. *Nat. Photonics* **2013**, *7*, 825–833.
19. Wang, H.Y.; Zheng, Y.F.; Zhang, L.; Yu, J.S. Effect of two-step annealing on the performance of ternary polymer solar cells based on P3HT:$PC_{71}$BM:SQ. *Sol. Energ. Mater. Sol. Cells* **2014**, *128*, 215–220.
20. Antoniadis, H.; Hsieh, B.R.; Abkowitz, M.A.; Jenekhe, S.A.; Stolka, M. Photovoltaic and photoconductive properties of aluminum/poly(p-phenylene vinylene) interface. *Synthetic Met.* **1994**, *62*, 265–271.
21. Riess, W.; Karg, S.; Dyakonov, V.; Meier, M.; Schwoerer, M. Electroluminescence and photovoltaic effect in PPV Schottky diodes. *J. Lumin.* **1994**, *60*, 906–911.
22. Hoppe, H.; Sariciftci, N.S. Organic solar cells: An overview. *J. Mater. Res.* **2004**, *19*, 1924–1945.
23. Tang, C.W. Two-layer organic photovoltaic cell. *Appl. Phys. Lett.* **1986**, *48*, 183–185.
24. Sariciftci, N.S.; Smilowitz, L.; Heeger, A.J.; Wudl, F. Photoinduced electron transfer from a conducting polymer to buckminsterfullerene. *Science* **1992**, *258*, 1474–1476.
25. Morita, S.; Zakhidov, A.A.; Yoshino, K. Doping effect of buckminsterfullerene in conducting polymer: Change of absorption spectrum and quenching of luminescene. *Solid State Commun.* **1992**, *82*, 249–252.
26. Sariciftci, N.S.; Smilowitz, L.; Heeger, A.J.; Wudl, F. Semiconducting polymers (as donors) and buckminsterfullerene (as acceptor): Photoinduced electron transfer and heterojunction device. *Synthetic Met.* **1993**, *59*, 333–352.
27. Yu, G.; Gao, J.; Hummelen, J.C.; Wudl, F.; Heeger, A.J. Polymer photovoltaic cells: Enhanced efficiencies via a network of internal donor-acceptor heterojunctions. *Science* **1995**, *270*, 1789–1791.
28. Halls, J.J.M.; Walsh, C.A.; Greenham, N.C.; Marseglia, E.A.; Friend, R.H.; Moratti, S.C.; Holmes, A.B. Efficient photodiodes from interpenetrating polymer network. *Nature* **1995**, *376*, 498–500.
29. Kim, Y.J.; Lee, K.; Coates, N.E.; Moses, D.; Nguyen, T.Q.; Dante, M.; Heeger, A.J. Efficient tandem polymer solar cells fabricated by all-solution processing. *Science* **2007**, *317*, 222–225.
30. Po, R.; Carbonera, C.; Bernardi, A.; Camaioni, N. The role of buffer layers in polymer solar cells. *Energ. Environ. Sci.* **2011**, *4*, 285–210.
31. Carle, J.E.; Andersen, T.R.; Helgesen, M.; Bundgaard, E.; Jorgensen, M.; Krebs, F.C. A laboratory scale approach to polymer solar cells using one coating/printing machine, flexible substrates, no ITO, no vacuum and no spincoating. *Sol. Energ. Mater. Sol. Cells* **2013**, *108*, 126–128.
32. Wang, Y.; Wei, W.; Liu, X.; Gu, X. Research progress on polymer heterojunction solar cells. *Sol. Energ. Mater. Sol. Cells* **2012**, *98*, 129–145.

33. Lewis, N.S. Toward cost-effective solar energy use. *Science* **2007**, *315*, 798–801.
34. Yu, J.S.; Wang, N.N.; Zang, Y.; Jiang, Y.D. Organic photovoltaic cells based on TPBi as a cathode buffer layer. *Sol. Energ. Mater. Sol. Cells* **2011**, *95*, 664–668.
35. Wang, N.N.; Yu, J.S.; Huang, J.; Jiang, Y.D. Effect of buffer layers on the performance of organic photovoltaic cells based on copper phthalocyanine and C60. *Sol. Energ. Mater. Sol. Cells* **2010**, *94*, 263–236.
36. Angmo, D.; Gevorgyan, S.A.; Larsen-Olsen, T.T.; Sondergaard, R.R.; Hosel, M.; Jorgensen, M.; Gupta, R.; Kulkarni, G.U.; Krebs, F.C. Scalability and stability of very thin, roll-to-roll processed, large area, indium-tin-oxide free polymer solar cell modules. *Org. Electron.* **2013**, *14*, 984–994.
37. Bundgaard, E.; Krebs, F.C. Low band gap polymers for organic photovoltaics. *Sol. Energ. Mater. Sol. Cells* **2007**, *91*, 954–985.
38. Muhlbacher, D.; Scharber, M.; Morana, M.; Zhu, Z.; Waller, D.; Gaudiana, R.; Brabec, C.J. High photovoltaic performance of a low-bandgap polymer. *Adv. Mater.* **2006**, *18*, 2884–2889.
39. Sun, Y.; Welch, G.C.; Leong, W.L.; Takacs, C.J.; Bazan, G.C.; Heeger, A.J. Solution-processed small-molecule solar cells with 6.7% efficiency. *Nat. Mater.* **2012**, *11*, 44–48.
40. Wu, C.; Murata, H. Thinking small for solar. *MRS Bull.* **2012**, *37*, 194–195.
41. Kyaw, A.K.K.; Wang, D.H.; Wynands, D.; Zhang, J.; Nguyen, T.Q.; Bazan, G.C.; Heeger, A.J. Improved light harvesting and improved efficiency by insertion of an optical spacer (ZnO) in solution-processed small-molecule solar cells. *Nano Lett.* **2013**, *13*, 3796–3801.
42. Ye, L.; Zhang, S.; Zhao, W.; Yao, H.; Hou, J. Highly efficient 2D-conjugated benzodithiophene-based photovoltaic polymer with linear alkylthio side chain. *Chem. Mater.* **2014**, *26*, 3603–3605.
43. Cui, C.; Wong, W.Y.; Li, Y. Improvement of open-circuit voltage and photovoltaic properties of 2D-conjugated polymers by alkylthio substitution. *Energ. Environ. Sci.* **2014**, *7*, 2276–2284.
44. Best Research-Cell Efficiencies. Available online: http://www.nrel.gov/ncpv/images/efficiency_chart.jpg (accessed on 15 July 2014).
45. Lee, M.M.; Teuscher, J.; Miyasaka, T.; Murakami, T.N.; Snaith, H.J. Efficient hybrid solar cells based on meso-superstructured organometal halide perovskites. *Science* **2012**, *338*, 643–647.
46. Liu, M.; Johnston, M.B.; Snaith, H.J. Efficient planar heterojunction perovskite solar cells by vapour deposition. *Nature* **2013**, *501*, 395–398.
47. Burschka, J. Sequential deposition as a route to high-performance perovskite-sensitized solar cells. *Nature* **2013**, *499*, 316–319.
48. Deibel, C.; Strobel, T.; Dyakonov, V. Role of the charge transfer state in organic donor–acceptor solar cells. *Adv. Mater.* **2010**, *22*, 4097–4111.
49. Strobel, T.; Deibel, C.; Dyakonov, V. Role of polaron pair diffusion and surface losses in organic semiconductor devices. *Phys. Rev. Lett.* **2010**, *105*, 266602.
50. Gélinas, S.; Paré-Labrosse, O.; Brosseau, C.N.; Albert-Seifried, S.; McNeill, C.R.; Kirov, K.R.; Howard, I.A.; Leonelli, R.; Friend, R.H.; Silva, C. The binding energy of charge-transfer excitons localized at polymeric semiconductor heterojunctions. *J. Phys. Chem. C* **2011**, *115*, 7114–7119.
51. Etzold, F.; Howard, I.A.; Mauer, R.; Meister, M.; Kim, T.D.; Lee, K.S.; Baek, N.S.; Laquai, F. Ultrafast exciton dissociation followed by nongeminate charge recombination in PCDTBT:PCBM photovoltaic blends. *J. Am. Chem. Soc.* **2011**, *133*, 9469–9479.

52. Morteani, A.C.; Sreearunothai, P.; Herz, L.M.; Friend, R.H.; Silva, C. Exciton regeneration at polymeric semiconductor heterojunctions. *Phys. Rev. Lett.* **2004**, *92*, 247402.
53. Grancini, G.; Maiuri, M.; Fazzi, D.; Petrozza, A.; Egelhaaf, H.J.; Brida, D.; Cerullo, G.; Lanzani, G. Hot exciton dissociation in polymer solar cells. *Nat. Mater.* **2013**, *12*, 29–33.
54. Shoaee, S.; Clarke, T.M.; Huang, C.; Barlow, S.; Marder, S.R.; Heeney, M.; McCulloch, I.; Durrant, J.R. Acceptor energy level control of charge photogeneration in organic donor/acceptor blends. *J. Am. Chem. Soc.* **2010**, *132*, 12919–12926.
55. Pensack, R.D.; Asbury, J.B. Barrierless free carrier formation in an organic photovoltaic material measured with ultrafast vibrational spectroscopy. *J. Am. Chem. Soc.* **2009**, *131*, 15986.
56. Bakulin, A.A.; Rao, A.; Pavelyev, V.G.; van Loosdrecht, P.H.; Pshenichnikov, M.S.; Niedzialek, D.; Cornil, J.; Beljonne, D.; Friend, R.H. The role of driving energy and delocalized states for charge separation in organic semiconductors. *Science* **2012**, *335*, 1340–1344.
57. Fu, G.; Yang, S.; Shi, J.; Zhang, Z.; Liu, B.; Zhao, X.; Li, G.; Li, X. Formation of charge-transfer complexes significantly improves the performance of polymer solar cells based on PBDTTT-C-T: PC71BM. *Prog. Photovoltaics* **2014**, doi:10.1002/pip.2509.
58. He, Z.; Zhong, C.; Su, S.; Xu, M.; Wu, H.; Cao, Y. Enhanced power-conversion efficiency in polymer solar cells using an inverted device structure. *Nat. Photonics* **2012**, *6*, 593–597.
59. Schlenker, C.W.; Chen, K.S.; Yip, H.L.; Li, C.Z.; Bradshaw, L.R.; Ochsenbein, S.T.; Ding, F.; Li, X.S.; Gamelin, D.R.; Jen, A.K.Y.; *et al.* Polymer triplet energy levels need not limit photocurrent collection in organic solar cells. *J. Am. Chem. Soc.* **2012**, *134*, 19661–19668.
60. Zhang, Y.; Zou, J.; Yip, H.L.; Chen, K.S.; Zeigler, D.F.; Sun, Y.; Jen, A.K.Y. Indacenodithiophene and quinoxaline-based conjugated polymers for highly efficient polymer solar cells. *Chem. Mater.* **2011**, *23*, 2289–2291.
61. Miller, N.C.; Sweetnam, S.; Hoke, E.T.; Gysel, R.; Miller, C.E.; Bartelt, J.A.; Xie, X.; Toney, M.F.; McGehee, M.D. Molecular packing and solar cell performance in blends of polymers with a bisadduct fullerene. *Nano Lett.* **2012**, *12*, 1566–1570.
62. Rao, A.; Chow, P.C.; Gelinas, S.C.; Schlenker, W.; Li, C.Z.; Yip, H.L.; Jen, A.K.Y.; Ginger, D.S.; Friend, R.H. The role of spin in the kinetic control of recombination in organic photovoltaics. *Nature* **2013**, *500*, 435–439.
63. Jamieson, F.C.; Domingo, E.B.; McCarthy-Ward, T.; Heeney, M.; Stingelin, N.; Durrant, J.R. *Chem. Sci.* **2012**, *3*, 485–492.
64. Savoie, B.M.; Rao, A.; Bakulin, A.A.; Gelinas, S.; Movaghar, B.; Friend, R.H.; Marks, T.J.; Ratner, M.A. Unequal partnership: asymmetric roles of polymeric donor and fullerene acceptor in generating free charge. *J. Am. Chem. Soc.* **2014**, *136*, 2876–2884.
65. Park, S.H.; Roy, A.; Beaupré, S.; Cho, S.; Coates, N.; Moon, J.S.; Moses, D.; Leclerc, M.; Lee, K.; Heeger, A.J. Bulk heterojunction solar cells with internal quantum efficiency approaching 100%. *Nat. Photonics* **2009**, *3*, 297–302.
66. Huang, J.; Yu, J.S.; Wang, W.; Jiang, Y.D. Organic solar cells with a multicharge separation structure consisting of a thin rubrene fluorescent dye for open circuit voltage enhancement. *Appl. Phys. Lett.* **2011**, *98*, 023301.

67. Huang, J.; Qi, Y.G.; Wang, H.Y.; Yu, J.S. Low roll off radiation efficiency of charge transfer state excitons based on organic photovoltaic and electroluminescent integrated device. *Appl. Phys. Lett.* **2013**, *102*, 183302.
68. Zang, Y.; Li, C.Z.; Chueh, C.C.; Williams, S.T.; Jiang, W.; Wang, Z.H.; Yu, J.S.; Jen, A.K.Y. Integrated molecular, interfacial, and device engineering towards high-performance non-fullerene based organic solar cells. *Adv. Mater.* **2014**, doi:10.1002/adma.201301992.
69. Liu, S.Q.; Wu, R.F.; Huang, J.; Yu, J.S. Color-tunable and high-efficiency organic light-emitting diode by adjusting exciton bilateral migration zone. *Appl. Phys. Lett.* **2013**, *103*, 133307.
70. Guan, Z.Q.; Yu, J.S.; Huang, J.; Zhang, L. Power efficiency enhancement of solution-processed small-molecule solar cells based on squaraine via thermal annealing and solvent additive methods. *Sol. Energ. Mater. Sol. Cells* **2013**, *109*, 262–269.
71. Hilczer, M.; Tachiya, M. Unified theory of geminate and bulk electron-hole recombination in organic solar cells. *J. Phys. Chem. C* **2010**, *114*, 6808–6813.
72. Braun, C.L. Electric field assisted dissociation of charge transfer states as a mechanism of photocarrier production. *J. Chem. Phys.* **1984**, *80*, 4157–4161.
73. Onsager, L. Initial recombination of ions. *Phys. Rev.* **1938**, *54*, 554–557.
74. Coffey, D.C.; Larson, B.W.; Hains, A.W.; Whitaker, J.B.; Kopidakis, N.; Boltalina, O.V.; Strauss, S.H.; Rumbles, G. An optimal driving force for converting excitons into free carriers in excitonic solar cells. *J. Phys .Chem. C* **2012**, *116*, 8916–8923.
75. Liu, T.; Troisi, A. Absolute rate of charge separation and recombination in a molecular model of the P3HT/PCBM interface. *J. Phys. Chem. C* **2011**, *115*, 2406–2415.
76. Wang, N.N.; Tong, X.; Burlingame, Q.; Yu, J.S.; Forrest, S.R. Photodegradation of small-molecule organic photovoltaics. *Sol. Energ. Mater. Sol. Cells* **2014**, *125*, 170–175.
77. .Huang, H.; Zhou, N.; Ortiz, R.P.; Chen, Z.; Loser, S.; Zhang, S.; Guo, X.; Casado, J.; Navarrete, T.L.; Yu, X.; *et al.* Alkoxy-functionalized thienyl-vinylene polymers for field-effect transistors and all-polymer solar cells. *Adv. Funct. Mater.* **2014**, *24*, 2782–2793.
78. Heeger, A.J. Bulk heterojunction solar cells: understanding the mechanism of operation. *Adv. Mater.* **2014**, *26*, 10–28.
79. Mayer, A.C.; Scully, S.R. Polymer-based solar cells. Mater. *Today* **2007**, *10*, 28–33.
80. Zhou, N.J.; Guo, X.G.; Ortiz, R.P.; Li, S.Q.; Zhang, S.M.; Chang, R.P.H.; Facchetti, A.; Marks, T.J. Bithiophene lmide and benzodithiophene copolymers for efficient inverted polymer solar cells. *Adv. Mater.* **2012**, *24*, 2242–2248.
81. Pandey, R.; Holmes, R.J. Graded donor-acceptor heterojunctions for efficient organic photovoltaic cells. *Adv. Mater.* **2012**, *22*, 5301–5305.
82. Deibel, C.; Dyakonov, V. Polymer-fullerene bulk heterojunction solar cells. *Rep. Prog. Phys.* **2010**, *73*, 096401.
83. Brday, M.A.; Su, G.M.; Chabinyc, M.L. Recent progress in the morphology of bulk heterojunction photovoltaics. *Soft. Matter.* **2011**, *7*, 11065–11077.
84. Aryal, M.; Buyukserin, F.; Mielczarek, K.; Zhao, X.M.; Gao, J.M.; Zakhidov, A.; Hu, W.C. Imprinted large-scale high density polymer nanopillars for organic solar cells. *Sci. Technol. B* **2008**, *26*, 2562–2566.

85. He, X.; Gao, F.; Tu, G.; Hasko, D.; Hüttner, S.; Steiner, U.; Greenham, N.C.; Friend, R.H.; Huck, W.T.S. Formation of nanopatterned polymer blends in photovoltaic devices. *Nano Lett.* **2010**, *10*, 1302–1307.
86. Steinhart, M.; Wendorff, J.H.; Greiner, A.; Wehrspohn, R.B.; Nielsch, K.; Schilling, J.; Choi, J.; Gösele, U. Wetting behaviors of hyperbranched polymer composites within ordered porous template under vibration. *Science* **2002**, *296*, 1997.
87. Steinhart, M.; Wehrspohn, R.B.; Gösele, U.; Wendorff, J.H. Nanotubes by template wetting: A modular assembly system. *Angew. Chem. Int. Ed.* **2004**, *43*, 1334–1344.
88. Moon, S.I.; McCarthy, T.J. Template synthesis and self-assembly of nanoscopic polymer pencils. *Macromolecules* **2003**, *36*, 4253–4255.
89. Feng, X.D.; Jin, Z.X. Spontaneous formation of nanoscale polymer spheres, capsules, or rods by evaporation of polymer solutions in cylindrical alumina nanopores. *Macromolecules* **2009**, *42*, 569–572.
90. Aryal, M.; Trivedi, K.; Hu, W.C. Nano-confinement induced chain alignment in ordered P3HT nanostructures defined by nanoimprint lithography. *ACS Nano* **2009**, *3*, 3085–3090.
91. Kim, J.S.; Park, Y.; Lee, D.Y.; Lee, J.H.; Park, J.H.; Kim, J.K.; Cho, K. Polymer controlled crystallization of unique mineral superstructures. *Adv. Funct. Mater.* **2010**, *20*, 540–545.
92. Wang, H.S.; Lin, L.H.; Chen, S.Y.; Wang, Y.L.; Wei, K.H. Ordered polythiophene/fullerene composite core-shell nanorod arrays for solar cell applications. *Nanotechnology* **2009**, *20*, 075201.
93. Chen, D.; Zhao, W.; Russell, T.P. P3HT nanopillars for organic photovoltaic devices nanoimprinted by AAO templates. *ACS Nano* **2012**, *6*, 1479–1485.
94. Moungthai, S.; Mahadevapuram, N.; Ruchhoeft, P.; Stein, G.E. Direct patterning of conductive polymer domains for photovoltaic devices. *ACS Appl. Mater. Inter.* **2012**, *4*, 4015–4023.
95. Tao, C.; Aljada, M.; Shaw, P.E.; Lee, K.H.; Cavaye, H.; Balfour, M.N.; Borthwick, R.J.; James, M.; Burn, P.L.; Gentle, I.R.; *et al*. Controlling hierarchy in solution-processed polymer solar cells based on crosslinked P3HT. *Adv. Energy Mater.* **2013**, *3*, 105–112.
96. Kim, J.B.; Kim, P.; Pegard, N.C.; Oh, S.J.; Kagan, C.R.; Fleischer, J.W.; Stone, H.A.; Loo, Y.L. Wrinkles and deep folds as photonic structures in photovoltaics. *Nat. Photonics* **2012**, *6*, 327–332.
97. Sun, Y.; Choi, W.M.; Jiang, H.; Huang, Y.Y.; Rogers, J.A. Controlled buckling of semiconductor nanoribbons for stretchable electronics. *Nat. Nanotechnol.* **2006**, *1*, 201–207.
98. Khang, D.Y.; Jiang, H.; Huang, Y.; Rogers, J.A. A stretchable form of single-crystal silicon for high- performance electronics on rubber substrates. *Science* **2006**, *311*, 208–212.
99. Rafael, B.; Pablo, R.G.; Alberto, M.O.; Xavier, E.; Marc, M.; Jordi, M. Transparent polymer solar cells employing a layered light-trapping architecture. *Nat. Photonics* **2013**, *7*, 995–1000.
100. Liu, J.; Namboothiry, M.A.G.; Carroll, D.L. Optical geometries for fiber-based organic photovoltaics. *Appl. Phys. Lett.* **2007**, *90*, 133515.
101. Silveirinha, M.G.; Alù, A.; Li, J.; Engheta, N. Nanoinsulators and nanoconnectors for optical nanocircuits. *J. Appl. Phys.* **2008**, *103*, doi:10.1063/1.2891423.
102. Li, Y.; Peterson, E.D.; Huang, H.; Wang, M.; Xue, D.; Nie, W.; Zhou, W.; Carroll, D.L. Tube-based geometries for organic photovoltaics. *Appl. Phys. Lett.* **2010**, *96*, 243505.

103. Liu, D.; Zhao, M.; Li, Y.; Bian, Z.; Zhang, L.; Shang, Y.; Xia, X.; Zhang, S.; Yun, D.; Liu, Z.; *et al.* Solid-state, polymer-based fiber solar cells with carbon nanotube electrodes. *ACS Nano* **2012**, *6*, 11027–11034.
104. Lee, M.R.; Eckert, R.D.; Forberich, K.; Dennler, G.; Brabec, C.J.; Gaudiana, R.A. Solar power wires based on organic photovoltaic materials. *Science* **2009**, *324*, 232–235.
105. Chen, T.; Qiu, L.; Li, H.; Peng, H. Polymer photovoltaic wires based on aligned carbon nanotube fibers. *J. Mater. Chem.* **2012**, *22*, 23655–23658.
106. Li, K.; Zhen, H.; Huang, Z.; Li, G.; Liu, X. Embedded surface relief gratings by a simple method to improve absorption and electrical properties of polymer solar cells. *ACS Appl. Mater. Inter.* **2012**, *4*, 4393–4397.
107. Lee, H.J.; Park, T.H.; Choi, J.H.; Song, E.H.; Shin, S.J.; Kim, H.; Choi, K.C.; Park, Y.W.; Ju, B.K. Negative mold transfer patterned conductive polymer electrode for flexible organic light-emitting diodes. *Org. Electron.* **2013**, *14*, 416–422.
108. Zheng, Y.F.; Li, S.G.; Yu, X.G.; Zheng, D.; Yu, J.S. Investigation of *in situ* annealing on poly(3,4-ethylenedioxythiophene):poly(styrenesulfonate): Towards all-solution processed inverted polymer solar cells. *RSC Advances* **2014**, *4*, 16464–16471.
109. Yang, X.N.; Loos, J.; Veenstra, S.C.; Verhees, W.J.H.; Wienk, M.M.; Kroon, J.M.; Michels, M.A.J.; Janssen, R.A.J. Nanoscale morphology of high-performance polymer solar cells. *Nano Lett.* **2005**, *5*, 579–583.
110. Erb, T.; Zhokhavets, U.; Gobsch, G.; Raleva, S.; Stuhn, B.; Schilinsky, P.; Waldauf, C.; Brabec, C.J. Correlation between structural and optical properties of composite polymer/fullerene films for organic solar cells. *Adv. Funct. Mater.* **2005**, *15*, 1193–1196.
111. Verploegen, E.; Mondal, R.; Betinger, C.J.; Sok, S.; Toney, M.F.; Bao, Z.N. Effects of thermal annealing upon the morphology of polymer–fullerene blends. *Adv. Funct. Mater.* **2005**, *20*, 3519–3529.
112. Zheng, Y.F.; Wu, R.F.; Shi, W.; Guan, Z.Q.; Yu, J.S. Effect of *in situ* annealing on the performance of spray coated polymer solar cells. *Sol. Energ. Mater. Sol. Cells* **2013**, *111*, 200–205.
113. Guan, Z.Q.; Wu, R.F.; Zang, Y.; Yu, J.S. Small molecule dye rubrene doped organic bulk heterojunction solar cells. *Thin Solid Films* **2013**, *539*, 278–283.
114. Shi, T.; Zhu, X.G.; Yang, D.; Xie, Y.H.; Zhang, J.; Tu, G.L. Thermal annealing influence on poly(3-hexyl-thiophene)/phenyl-C61-butyric acid methyl ester-based solar cells with anionic conjugated polyelectrolyte as cathode interface layer. *Appl. Phys. Lett.* **2012**, *101*, doi:10.1063/1.4759148.
115. Sirringhaus, H.; Tessler, H.; Friend, R.H. Integrated optoelectronic devices based on conjugated polymers. *Science* **1998**, *280*, 1741–1744.
116. Kline, R.J.; McGehee, M.D.; Kadnikova, E.N.; Liu, J.; Fréchet, J.M.J.; Toney, M.F. Dependence of regioregular poly(3-hexylthiophene) film morphology and field-effect mobility on molecular weight. *Macromolecules* **2005**, *38*, 3312–3319.
117. Oklobia, O.; Shafai, T.S. A quantitative study of the formation of PCBM clusters upon thermal annealing of P3HT/PCBM bulk heterojunction solar cell. Sol. *Energ. Mater. Sol. Cells* **2013**, *117*, 1–8.

118. Tsoi, W.C.; James, D.T.; Domingo, E.B.; Kim, J.S.; Al-Hashimi, M.; Murphy, C.E.; Stingelin, N.; Heeney, M.; Kim, J.S. Effects of a heavy atom on molecular order and morphology in conjugated polymer:fullerene photovoltaic blend thin films and devices. *ACS Nano* **2012**, *6*, 9646–9656.
119. Ng, A.; Liu, X.; To, C.H.; Djurišić, A.B.; Zapien, J.A.; Chan, W.K. Annealing of P3HT:PCBM blend film-the effect on its optical properties. *ACS Appl. Mater. Inter.* **2013**, *5*, 4247–4259.
120. Zhao, C.; Qiao, X.; Chen, B.; Hu, B. Thermal annealing effect on internal electrical polarization in organic solar cells. *Org. Electron.* **2013**, *14*, 2192–2197.
121. Shih, C.F.; Hung, D.T.; Wu, H.T.; Fu, S.W.; Chen, H.J.; Hsiao, C.Y. *In situ* monitoring of photovoltaic properties in organic solar cells during thermal annealing. *Org. Electron.* **2012**, *13*, 373–376.
122. Wodo, O.; Tirthapura, S.; Chaudhary, S.; Ganapathysubramanian, B. A graph-based formulation for computational characterization of bulk heterojunction morphology. *Org. Electron.* **2012**, *13*, 1105–1113.
123. Domanski, A.L.; Lieberwirth, I.; Sengupta, E.; Landfester, K.; Butt, H.J.; Berger, R.; Dyakonov, V.; Deibel, C. Effect of morphological changes on presence of trap states in P3HT:PCBM solar cells studied by cross-sectional energy filtered TEM and thermally stimulated current measurements. *J. Phys. Chem. C* **2013**, *117*, 23495–23499.
124. Nieuwendaal, R.C.; Ro, H.W.; Germack, D.S.; Kline, R.J.; Toney, M.F.; Chan, C.K.; Agrawal, A.; Gundlach, D.; VandeHart, D.L.; Delongchamp, D.M. Measuring domain sizes and compositional heterogeneities in P3HT-PCBM bulk heterojunction thin films with 1H spin diffusion NMR spectroscopy. *Adv. Funct. Mater.* **2012**, *22*, 1255–1266.
125. Keivanidis, P.E.; Kamm, V.; Zhang, W.; Floudas, G.; Laquai, F.; McCulloch, I.; Bradley, D.C.; Nelson, J. Correlating emissive non-geminate charge recombination with photocurrent generation efficiency in polymer/perylene diimide organic photovoltaic blend films. *Adv. Funct. Mater.* **2012**, *22*, 2318–2326.
126. Gu, Y.; Wang, C.; Russell, T.P. Multi-length-scale morphologies in PCPDTBT/PCBM bulk-heterojunction solar cells. *Adv. Energ. Mater.* **2012**, *2*, 683–690.
127. Street, R.A.; Krakaris, A.; Cowan, S.R. Recombination through different types of localized states in organic solar cells. *Adv. Funct. Mater.* **2012**, *22*, 4608–4619.
128. Wang, T.; Pearson, A.J.; Dunbar, A.D.F.; Staniec, P.A.; Watters, D.C.; Yi, H.; Ryan, A.J.; Jones, R.A.L.; Iraqi, A.; Lidzey, D.G. Correlating structure with function in thermally annealed PCDTBT:PC70BM photovoltaic blends. *Adv. Funct. Mater.* **2012**, *22*, 1399–1408.
129. Bertho, S.; Janssen, G.; Cleij, T.J.; Conings, B.; Moons, W.; Gadisa, A.; D'Haen, J.; Goovaerts, E.; Lutsen, L.; Manca, J.; *et al.* Effect of temperature on the morphological and photovoltaic stability of bulk heterojunction polymer:fullerene solar cells. *Sol. Energ. Mater. Sol. Cells* **2008**, *92*, 753–760.
130. Swinnen, A.; Haeldermans, I.; Ven, M.; D'Haen, J.; Vanhoyland, G.; Aresu, S.; D'Olieslaeger, M.; Manca, J. Tuning the dimensions of C60-based needlelike crystals in blended thin films. *Adv. Funct. Mater.* **2006**, *16*, 760–765.
131. Hoppe, H.; Sariciftci, N.S. Morphology of polymer/fullerene bulk heterojunction solar cells. *J. Mater. Chem.* **2006**, *16*, 45–61.

132. Tang, H.; Lu, G.; Li, L.; Li, J.; Wang, Y.; Yang, X. Precise construction of PCBM aggregates for polymer solar cells via multi-step controlled solvent vapor annealing. *J. Mater. Chem.* **2010**, *20*, 683–688.
133. Savenjie, T.J.; Kroeze, J.E.; Yang, X.; Loos, J. The effect of thermal treatment on the morphology and charge carrier dynamics in a polythiophene–fullerene bulk heterojunction. *Adv. Funct. Mater.* **2005**, *15*, 1260–1266.
134. Wu, W.R.; Jeng, U.S.; Su, C.J.; Wei, K.H.; Su, M.S.; Chiu, M.Y.; Chen, C.Y.; Su, W.B.; Su, C.H.; Su, A.C. Competition between fullerene aggregation and poly(3-hexylthiophene) crystallization upon annealing of bulk heterojunction solar cells. *ACS Nano* **2011**, *5*, 6233–6243.
135. Chen, H.; Hu, S.; Zang, H.; Hu, B.; Dadmun, M. Precise structural development and its correlation to function in conjugated polymer: fullerene thin films by controlled solvent annealing. *Adv. Funct. Mater.* **2013**, *23*, 1701–1710.
136. Zhang, W.; Hu, R.; Li, D.; Huo, M.M.; Ai, X.C.; Zhang, J.P. Primary dynamics of exciton and charge photogeneration in solvent vapor annealed P3HT/PCBM films. *J. Phys. Chem. C* **2012**, *116*, 4298–4310.
137. Bull, T.A.; Pingree, L.S.C.; Jenekhe, S.A.; Ginger, D.S.; Luscombe, C.K. The role of mesoscopic PCBM crystallites in solvent vapor annealed copolymer solar cells. *ACS Nano* **2009**, *3*, 627–636.
138. Nam, S.; Jang, J.; Cha, H.; Hwang, J.; An, T.K.; Park, S.; Park, C.E. Effects of direct solvent exposure on the nanoscale morphologies and electrical characteristics of PCBM-based transistors and photovoltaics. *J. Mater. Chem.* **2012**, *22*, 5543–5549.
139. Verploegen, E.; Miller, C.E.; Schmidt, K.; Bao, Z.; Toney, M.F. Manipulating the morphology of P3HT–PCBM bulk heterojunction blends with solvent vapor annealing. *Chem. Mater.* **2012**, *24*, 3923–3931.
140. Huang, Y.C.; Chia, H.C.; Chuang, C.M.; Tsao, C.S.; Chen, C.Y.; Su, W.F. Facile hot solvent vapor annealing for high performance polymer solar cell using spray process. *Sol. Energ. Mater. Sol. Cells* **2013**, *114*, 24–30.
141. Li, H.; Tang, H.L.; Xu, W.; Zhao, X.; Yang, X. Solvent-soaking treatment induced morphology evolution in P3HT/PCBM composite films. *J. Mater. Chem.* **2011**, *21*, 6563–3568.
142. Jeon, J.H.; Lee, H.K.; Wang, D.H.; Park, J.H.; Park, O.O. The role of non-solvent swelling in bulk hetero junction solar cells. *Sol. Energ. Mater. Sol. Cells* **2012**, *102*, 196–200.
143. Zhou, H.; Zhang, Y.; Seifter, J.; Collins, S.D.; Luo, C.; Bazan, G.C.; Nguyen, T.Q.; Heeger, A.J. High-efficiency polymer solar cells enhanced by solvent treatment. *Adv. Mater.* **2013**, *25*, 1646–1652.
144. Lee, B.R.; Jung, E.D.; Nam, Y.S.; Jung, M.; Park, J.S.; Lee, S.; Choi, H.; Ko, S.J.; Shin, N.R.; Kim, Y.K.; *et al*. Amine-based polar solvent treatment for highly efficient inverted polymer solar cells. *Adv. Mater.* **2014**, *26*, 494–500.
145. Qu, B.; Tian, D.; Cong, Z.; Wang, W.; An, Z.; Gao, C.; Gao, Z.; Yang, H.; Zhang, L.; Xiao, L.; *et al.* Highly efficient solar cells based on the copolymer of benzodithiophene and thienopyrroledione with solvent annealing. *J. Phys. Chem. C* **2013**, *117*, 3272–3278.
146. Sharma, G.D.; Suresh, P.; Sharma, S.S.; Vijay, Y.K.; Mikroyannidis, J.A. Effect of solvent and subsequent thermal annealing on the performance of Phenylenevinylene copolymer:PCBM solar cells. *ACS Appl. Mater. Inter.* **2010**, *2*, 504–510.

147. Gholamkhass, B.; Servati, P. Solvent-vapor induced morphology reconstruction for efficient PCDTBT based polymer solar cells. *Org. Electron.* **2013**, *14*, 2278–2283.
148. Peet, J.; Solci, C.; Coffin, R.C.; Nguyen, T.Q.; Mikhailovsky, A.; Moses, D.; Bazan, G.C. Method for increasing the photoconductive response in conjugated polymer/fullerene composites. *Appl. Phys. Lett.* **2006**, *40*, 13353.
149. Peet, J.; Kim, J.Y.; Coates, N.E.; Ma, W.L.; Moses, D.; Heeger, A.J.; Bazan, G.C. Efficiency enhancement in low-bandgap polymer solar cells by processing with alkane dithiols. *Nat. Mater.* **2007**, *6*, 497–500.
150. Li, G.; Yao, Y.; Yang, H.; Shrotriya, V.; Yang, G.; Yang, Y. Solvent annealing effect in polymer solar cells based on Poly(3-hexylthiophene) and methanofullerenes. *Adv. Funct. Mater.* **2007**, *17*, 1636–1644.
151. Salim, T.; Wong, L.H.; Brauer, B.; Kukreja, R.; Foo, Y.L.; Bao, Z.N.; Lam, Y.M. Solvent additives and their effects on blend morphologies of bulk heterojunctions. *J. Mater. Chem.* **2011**, *21*, 242–250.
152. Lee, J.K.; Ma, W.L.; Brabec, C.J.; Yuen, J.; Moon, J.S.; Kim, J.Y.; Lee, K.; Bazan, G.C.; Hegger, A.J. Processing additives for improved efficiency from bulk heterojunction solar cells. *J. Am. Chem. Soc.* **2008**, *130*, 3619–3623.
153. Szarko, J.M.; Guo, J.; Liang, Y.; Lee, B.; Rolczynski, B.S.; Strzalka, J.; Xu, T.; Loser, S.; Marks, T.J.; Yu, L.; *et al.* When function follows form: effects of donor copolymer side chains on film morphology and BHJ solar cell performance. *Adv. Mater.* **2010**, *22*, 5468–5472.
154. Li, T.; Hu, W.; Zhu, D. Contents. *Adv. Mater.* **2010**, *22*, 135–138.
155. Yang, J.S.; Oh, S.H.; Kim, D.L.; Kim, S.J.; Kim, H.J. Hole transport enhancing effects of polar solvents on poly(3,4-ethylenedioxythiophene):poly(styrene sulfonic acid) for organic solar cells. *ACS Appl. Mater. Interfaces* **2012**, *4*, 5394–5398.
156. Zhang, Y.; Li, Z.; Wakim, S.; Alem, S.; Tsang, S.W.; Lu, J.; Ding, J.; Tao, Y. Bulk heterojunction solar cells based on a new low-band-gap polymer: Morphology and performance. *Org. Electron.* **2011**, *12*, 1211–1215.
157. Lou, S.J.; Szarko, J.M.; Xu, T.; Yu, L.; Marks, T.J.; Chen, L.X. Effects of additives on the morphology of solution phase aggregates formed by active layer components of high-efficiency organic solar cells. *J. Am. Chem. Soc.* **2011**, *133*, 20661–20663.
158. Wang, D.H.; Pron, A.; Leclerc, M.; Heeger, A.J. Additive-Free bulk-heterojuction solar cells with enhanced power conversion efficiency, comprising a newly designed selenophene-thienopyrrolodione copolymer. *Adv. Funct. Mater.* **2013**, *23*, 1297–1304.
159. Ye, L.; Zhang, S.; Qian, D.; Wang, Q.; Hou, J. Application of bis-PCBM in polymer solar cells with improved voltage. *J. Phys. Chem. C* **2013**, *117*, 25360–25366.
160. Dou, L.; Gao, J.; Richard, E.; You, J.; Chen, C.C.; Cha, K.C.; He, Y.; Li, G.; Yang, Y. Systematic investigation of benzodithiophene and diketopyrrolopyrrole-based low-bandgap polymers designed for single junction and tandem polymer solar cells. *J. Am. Chem. Soc.* **2012**, *134*, 10071–10079.
161. Do, T.T.; Ha, Y.E.; Kim, J.H. Effect of the number of thiophene rings in polymers with 2,1,3-benzooxadiazole core on the photovoltaic properties. *Org. Electron.* **2013**, *14*, 2673–2681.

162. Etzold, F.; Howard, I.A.; Forler, N.; Cho, D.M.; Meister, M.; Mangold, H.; Shu, J.; Hansen, M.R.; Müllen, K.; Laquai, F. The Effect of solvent additives on morphology and excited-state dynamics in PCPDTBT:PCBM photovoltaic blends. *J. Am. Chem. Soc.* **2012**, *134*, 10569–10583.
163. Seo, J.H.; Nam, S.Y.; Lee, K.S.; Kim, T.D.; Cho, S. The effect of processing additive on aggregated fullerene derivatives in bulk-heterojunction polymer solar cells. *Org. Electron.* **2012**, *13*, 570–578.
164. Ramani, R.; Alam, S. A comparative study on the influence of alkyl thiols on the structural transformations in P3HT/PCBM and P3OT/PCBM blends. *Polymer* **2013**, *54*, 6785–6792.
165. Aïch, B.R.; Lu, J.; Beaupré, S.; Leclerc, M.; Tao, Y. Control of the active layer nanomorphology by using co-additives towards high-performance bulk heterojunction solar cells. *Org. Electron.* **2012**, *13*, 1736–1741.
166. Chang, L.; Jacobs, I.E.; Augustine, M.P.; Moulé, A.J. Correlating dilute solvent interactions to morphology and OPV device performance. *Org. Electron.* **2013**, *14*, 2431–2443.
167. Huang, J.S.; Goh, T.; Li, X.; Sfeir, M.Y.; Bielinski, E.A.; Tomasulo, S.; Lee, M.L.; Hazari, N.; Taylor, A.D. Polymer bulk heterojunction solar cells employing Förster resonance energy transfer. *Nat. Photonics* **2013**, *7*, 479–485.
168. Cho, Y.J.; Lee, J.Y.; Chin, B.D.; Forrest, S.R. Polymer bulk heterojunction photovoltaics employing a squaraine donor additive. *Org. Electron.* **2013**, *14*, 1081–1085.
169. Lobez, J.M.; Andrew, T.L.; Bulović, V.; Swager, T.M. Improving the performance of P3HT–Fullerene solar cells with side-chain-functionalized Poly(thiophene) additives: A new paradigm for polymer design. *ACS Nano* **2012**, *6*, 3044–3056.
170. Min, J.; Luponosov, Y.N.; Ameri, T.; Elschner, A.; Peregudova, S.M.; Baran, D.; Heumuuler, T.; Li, N.; Machui, F.; Ponomarenko, S.; *et al.* A solution-processable star-shaped molecule for high-performance organic solar cells via alkyl chain engineering and solvent additive. *Org. Electron.* **2013**, *14*, 219–229.
171. Liu, X.; Huettner, S.; Rong, Z.; Sommer, M.; Friend, R.H. Solvent additive control of morphology and crystallization in semiconducting polymer blends. *Adv. Mater.* **2012**, *24*, 669–674.
172. Zhang, Y.; Zhou, H.; Seifter, J.; Ying, L.; Mikailovsky, A.; Heeger, A.J.; Bazan, G.C.; Nguyen, T.Q. Molecular doping enhances photoconductivity in polymer bulk heterojunction solar cells. *Adv. Mater.* **2013**, *25*, 7038–7044.
173. Lu, L.; Xu, T. The role of N-Doped multiwall carbon nanotubes in achieving highly efficient polymer bulk heterojunction solar cells. *Nano Lett.* **2013**, *13*, 2365–2369.
174. Chen, M.C.; Kar, S.; Liaw, D.J.; Chen, W.H.; Huang, Y.C.; Tai, Y. Small organic additive to improve the charge separation in an inverted bulk heterojunction organic photovoltaic. *Org. Electron.* **2012**, *13*, 2702–2708.
175. Chen, H.Y.; Lan, S.; Yang, P.C.; Lin, S.H.; Sun, J.Y.; Lin, C.F. Poly(3-hexylthiophene):indene-C60 bisadduct morphology improvement by the use of polyvinylcarbazole as additive. *Sol. Energ. Mater. Sol. Cells* **2013**, *113*, 90–95.
176. Huang, J.; Zhan, C.; Zhang, X.; Zhao, Y.; Lu, Z.; Jia, H.; Jiang, B.; Ye, J.; Zhang, S.; Tang, A.; *et al.* Solution-processed DPP-based small molecule that gives high photovoltaic efficiency with judicious device optimization. *ACS Appl. Mater. Inter.* **2013**, *5*, 2033–2039.

177. Li, K.; Li, Z.; Feng, K.; Xu, X.; Wang, L.; Peng, Q. Development of large band-gap conjugated copolymers for efficient regular single and tandem organic solar cells. *J. Am. Chem. Soc.* **2013**, *135*, 13549–13557.
178. Aich, B.R.; Beaupre, S.; Leclerc, M.; Tao, Y. Highly efficient thieno[3,4-c]pyrrole-4,6-dione-based solar cells processed from non-chlorinated solvent. *Org. Electron.* **2014**, *15*, 543–548.
179. Chen, K.S.; Yip, H.L.; Schlenker, C.W.; Ginger, D.S.; Jen, A.K.Y. Halogen-free solvent processing for sustainable development of high efficiency organic solar cells. *Org. Electron.* **2012**, *13*, 2870–2878.
180. Sharma, G.D.; Singh, S.P.; Roy, M.S.; Mikroyannidis, J.A. Solution processed bulk heterojunction polymer solar cells with low band gap DPP-CN small molecule sensitizer. *Org. Electron.* **2012**, *13*, 1756–1762.
181. Lai, Y.C.; Higashihara, T.; Hsu, J.C.; Ueda, M.; Chen, W.C. Enhancement of power conversion efficiency and long-term stability of P3HT/PCBM solar cells using C60 derivatives with thiophene units as surfactants. *Sol. Energ. Mater. Sol. Cells* **2012**, *97*, 164–170.
182. Giebink, N.C.; Wiederrecht, G.P.; Wasielewski, M.R.; Forrest, S.R. Thermodynamic efficiency limit of excitonic solar cells. *Phys. Rev. B* **2011**, *83*, 195326.